

OPEN ACCESS

EDITED BY Hao Wang, Chinese Academy of Sciences (CAS), China

REVIEWED BY Ling Ren, Chinese Academy of Sciences (CAS), China Farzad Badkoobeh, University of Tehran, Iran Wolfdietrich Meyer,

Fraunhofer Institute for Applied Polymer

*CORRESPONDENCE Yaohua Li.

liyh@ydcmdei.org.cn
 iyh@ydcmdei.org.cn

Research (FHG), Germany

RECEIVED 10 August 2025 ACCEPTED 24 September 2025 PUBLISHED 23 October 2025

CITATION

Jiang S, Zhang J, Tian T, You M, Qu C and Li Y (2025) 3D printing of magnesium-containing biomedical materials for bone repairment towards actual applications. Front. Mater. 12:1682972. doi: 10.3389/fmats.2025.1682972

COPYRIGHT

© 2025 Jiang, Zhang, Tian, You, Qu and Li. This is an open-access article distributed under the terms of the Creative Commons Attribution License (CC BY). The use, distribution or reproduction in other forums is permitted, provided the original author(s) and the copyright owner(s) are credited and that the original publication in this journal is cited, in accordance with accepted academic practice. No use, distribution or reproduction is permitted which does not comply with these terms.

3D printing of magnesium-containing biomedical materials for bone repairment towards actual applications

Shan Jiang¹, Jiazhen Zhang², Tian Tian¹, Mingyu You¹, Chunge Qu¹ and Yaohua Li¹*

¹Yangtze River Delta Center for Medical Device Evaluation and Inspection, National Medical Products Administration of China, Beijing, China, ²Center for Medical Device Evaluation, National Medical Products Administration of China, Beijing, China

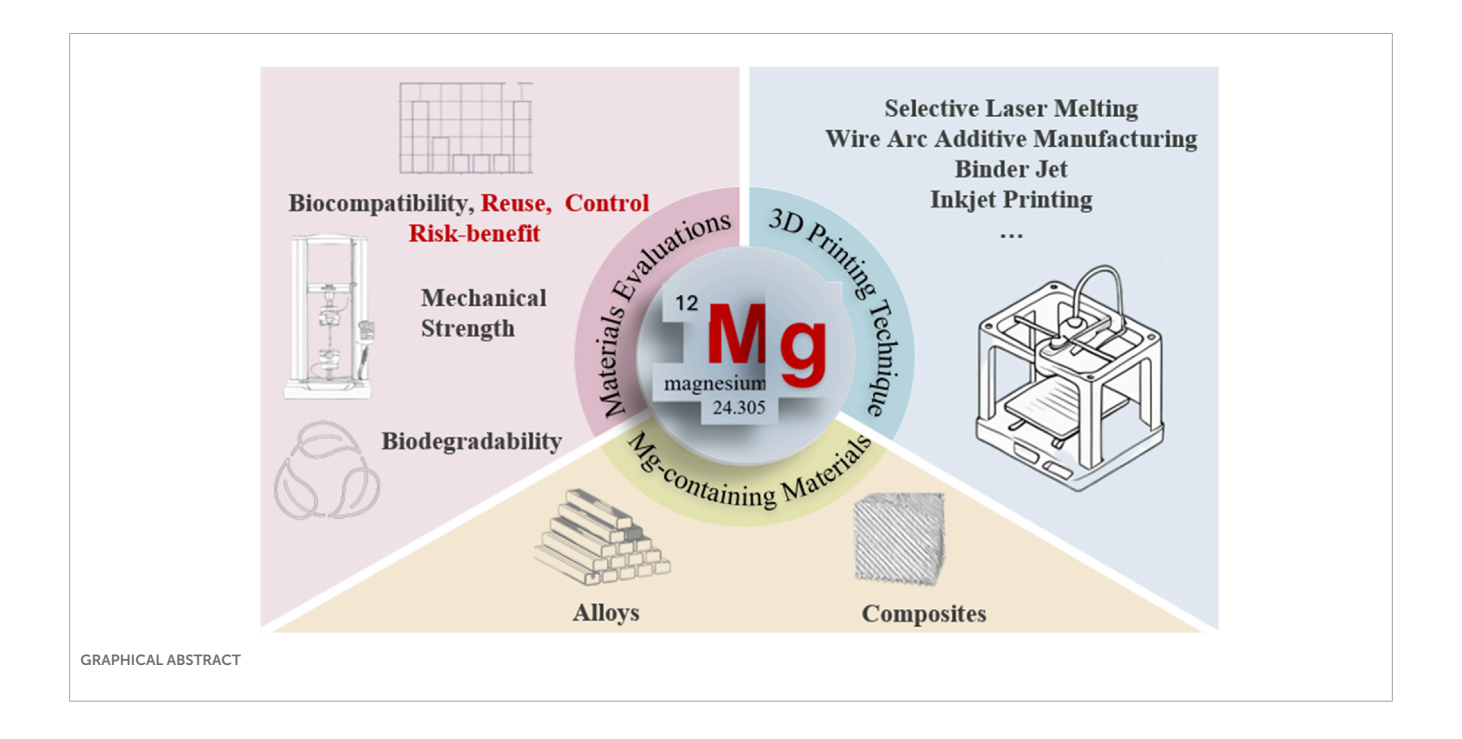
The integration of biodegradable magnesium (Mg)-containing materials with additive manufacturing technologies has opened promising avenues for next-generation biomedical implants. Owing to their unique combination of biodegradability and mechanical compatibility with bone, Mg alloys and composites have emerged as candidates for temporary orthopedic and cardiovascular devices. This review critically examines recent progress in 3D printing of Mg-containing biomaterials, with a focus on material design, fabrication strategies, and translational pathways toward clinical application. We analyze the performance of leading additive manufacturing techniques-including Selective Laser Melting (SLM), Wire Arc Additive Manufacturing (WAAM), Binder Jetting (BJAM), and 3D Gel Printing (3DGP) in tailoring biocompatibility and mechanical behavior to meet clinical demands. Beyond conventional material assessments, this review also identifies critical challenges in evaluating customized 3D printed implants, emphasizing the need for adapted regulatory and testing frameworks. By mapping advances from laboratory research to clinical translation, this review underscores the transformative potential of 3D printing Mg-containing biodegradable implants in bone repair. With their advantages to provide temporary support, stimulate osteogenesis, and gradually resorb without secondary surgery, Mg-containing constructs represent a cornerstone for the future of customized and sustainable implant technologies.

KEYWORDS

3D-printing, magnesium, additive manufacturing, Mg-containing, bone repair

1 Introduction

Given the significance of individual variations, 3D printing technology has emerged as a critical tool in advanced therapeutics (Zhu et al., 2025; Tetsuka and Shin, 2020; Kumar Pankaj et al., 2021; Wang et al., 2016; Ngo et al., 2018; Gu et al., 2012; Kaur and Singh, 2019; Roseti et al., 2017; Murphy and Atala, 2014). By utilizing patient-specific CT or MRI scan data, 3D printing technology enables



the design and fabrication of customized implants or scaffolds that precisely match the anatomical structure and clinical requirements of individual patients. Currently, titanium alloys (Sheng et al., 2022; Guo et al., 2022), stainless steel (Mahajan et al., 2023; Liang et al., 2023), and cobalt-chromium (Mahajan et al., 2023; Liang et al., 2023; Sing et al., 2016) alloys are widely adopted as 3D-printing materials for orthopedic and dental implants due to their superior mechanical properties and biocompatibility.

Very recently, biodegradable alloys such as iron (Fe), zinc (Zn), and magnesium (Mg) have been drawn great attention (Ngo et al., 2018; Mahajan et al., 2023; Liang et al., 2023). Unlike inert metals, they are designed to gradually degrade in the physiological environment, ultimately being absorbed or metabolized by the body. This degradation eliminates the need for secondary removal surgery and reduces long-term complications associated with stress shielding. It also provides a temporary mechanical function that aligns with the tissue healing process.

Amongst biodegradable metals, Fe and Zn based biomaterials have demonstrated favorable corrosion stability and biocompatibility (Qin et al., 2019; Kumar Rakesh et al., 2021). Fe alloys exhibit high mechanical strength but degrade too slowly, which limits their timely resorption *in vivo*. Conversely, Zn alloys offer moderate degradation rates and promising antibacterial effects, yet their relatively low strength and ductility restrict their applications in load-bearing environments.

Mg and its alloys and composites stand out as the most promising candidates for clinical translation because of their unique combination of properties (Liang et al., 2023; Qin et al., 2019; Kumar Rakesh et al., 2021; Karunakaran et al., 2020; Li et al., 2018; Nabiyouni et al., 2018; Manakari et al., 2017). As a naturally occurring element in the human body, Mg exhibits exceptional biocompatibility to harmonize metabolically with calcium and other physiological components. Notably, Mg-containing alloys and composites possess inherent biodegradability, allowing gradual

degradation *in vivo* and eliminating the need for secondary surgical removal. Furthermore, the degradation process releases hydrogen gas, creating a highly alkaline microenvironment that has been proved to enhance osteogenesis. Mechanically, Mg-containing alloys and composites demonstrate elastic moduli closer to those of natural bone tissue compared to traditional titanium or stainless-steel implants, thereby reducing stress shielding effects and mitigating risks of bone resorption. These facilitates Mg-containing materials as potential candidates for hard tissue regeneration.

To fully harness the potential of biodegradable metals, advanced manufacturing (AM) technologies, particularly 3D printing have played a pivotal role. Unlike conventional fabrication methods, AM enables precise control over implant geometry, porosity and internal architecture, facilitating the design of customized implants tailored to individual anatomical and mechanical needs. Moreover, 3D printing allows integration of material and structural optimization, enabling the fine tuning of mechanical strength and degradation behavior. As the degradation rate and mechanical reliability are critical for Mg-containing biomaterials, 3D printing provides a powerful platform to engineer structure and function that could enhance osteointegration while maintaining structural integrity during healing. As such, the convergence of biodegradable Mg-based materials with advanced manufacturing represents a paradigm shift in the development of next-generation biomedical implants.

However, current 3D-printing magnesium-containing biomedical materials still face multiple challenges towards actual use. The challenges mainly lie in its high chemical reactivity, low physical strength and the often-neglected manufacturing and evaluation process, as the individual variability in customized device may need further assessment in customized manufacturing and individual compatibility.

Based upon the above discussions, it is worthwhile to review both material and manufacturing progress in 3D Printing of

Mg-containing biomedical materials. To realize this purpose, we concluded its translational trajectory from material development to practical clinical applications. We critically examined the advancements in materials design and 3D fabrication techniques, with special emphasis focusing on evaluating the customized biomedical materials and devices. We hope this review would help bridge current gap between laboratory-scale innovations and clinically viable solutions, addressing both technical challenges and fabrication considerations for its actual commercialization.

2 Classification of 3D-printing Mg-containing biomedical materials

Currently, 3D-printing Mg-containing biomedical materials can be categorized into two primary systems: Mg-containing metallic materials and Mg-containing composite materials.

2.1 Mg-containing metallic materials

Pure magnesium, despite its low density of 1.74 g/cm³, suffers from inadequate tensile strength and poor corrosion resistance compared to conventional engineering alloys. Consequently, 3Dprinting magnesium materials are predominantly developed as magnesium alloys or composite systems to enhance corrosion resistance. In perspective of Mg alloys, they are typically synthesized by alloying with rare earth elements such as RE, Ce, Y or other metal elements such as Ca, Zr, Sr, Zn and Al. These additions are designed to refine grain size, modulate internal stresses, phase distribution and metal microstructures, thereby improving the material mechanical and corrosion properties. So far, established alloy systems mainly include Mg-RE-Zr (WE series), Mg-RE-Zn (EZ series), Mg-Zn-Zr (ZK series), Mg-Al-Mn (AM series), Mg-Al-RE (AE series), and Mg-Al-Zn (AZ series). All series have been demonstrated of their advantages for biomedical usage. The WE series, exemplified by WE43, offers superior degradation control with rates as low as 0.2 mm/year due to stable oxide layers formed by rare earth elements like Y and Nd, making it suitable for longterm implants such as load-bearing bone plates and cardiovascular stents. Additionally, Y3+ ions could enhance osteointegration by promoting bone mineralization density up to 30% increase in vitro (Liu Bingchuan et al., 2024; Min et al., 2023). The EZ series achieves an optimal balance between mechanical strength and degradation resistance, where Zn provides solid solution strengthening while REs mitigate localized corrosion, resulting in 40% less hydrogen cavity formation compared to AZ alloys (Salehi et al., 2019). ZK series alloys such as ZK60, exhibit exceptional biocompatibility of cell viability >95% owing to the presence of physiological elements Zr⁴⁺ and antibacterial Zn²⁺. When coupled with high tensile strength up to 350 MPa, it is ideal for orthopedic load-bearing devices (Xie et al., 2024). The AM series, namely AM60, demonstrates outstanding biosafety with well-defined metabolic pathways for Al³⁺/Mn²⁺, facilitating rapid endothelialization for cardiovascular applications (Rezanezhad and Azadi, 2024; Beyzavi et al., 2023). AE series alloys such as AE44, feature refined β-Mg₁₇Al₁₂ phases via RE additions, reducing pitting corrosion depth by 60% versus AZ91. It also enables uniform degradation and offers a cost-effective solution for medium-term implants such as dental screws with low RE content of <2%. The AZ series leverages $\rm Zn^{2+}$ to accelerate bone healing by 20%–30% through upregulation of Runx2/RANKL pathways and benefits from near-net-shaping capabilities for fabricating porous bone scaffolds, although its rapid degradation necessitates further surface modifications (Salehi et al., 2023a; Hartmann et al., 2024).

To take one step further, currently scientists manage to integrate alloy design principles with 3D-printing requirements or to balance the degradation kinetics and mechanical strengthening compatibility with tissue response. As depicted in Figures 1a,b, Chen et al. fabricated porous Mg-1Zn-1Ca-0.5 Mn (LP-ZMX101) scaffolds via melt infiltration into Ti scaffolds followed by mold removal (Yu et al., 2024). The LP-ZMX101 alloy exhibited extended hydrogen evolution duration of approximately 200 h owing to the continuous reticular secondary phases acting as corrosion barriers (Figure 1c). These scaffolds demonstrated exceptional biocompatibility and non-cytotoxicity, supporting their clinical viability. Mohammad et al. developed mechanically strengthened Mg-2Zn-0.2Ag screws (Figure 1d) through solvothermal processing combined with multi-directional forging to regulate the material microstructure (Asadollahi et al., 2024). The alloy achieved an ultimate shear strength of 149.5 MPa, with enhanced corrosion resistance via phosphate layer formation in PBS. Cell adhesion and viability were also significantly improved compared to pure Mg. Long et al. alternatively employed first-principles calculations and experimental phase diagrams to identify the novel ternary Mg41 (Gd,Sr)5 alloy in Figure 1e. Their work established a comprehensive mechanical-thermodynamic database for Mg-Gd-Sr systems, accelerating the development of high-performance Mg-containing alloys for biomedical devices (Long et al., 2023).

2.2 Mg-containing composite materials

Besides Magnesium alloy, recent innovations have been extended to the field of Mg-containing composites, which could address both limitations of Mg and polymers/ceramics while enabling controlled Mg²⁺ release to stimulate osteogenesis and suppress inflammation. In 2021, Lin et al. designed a porous Mg scaffold using magnesium powder-reinforced epoxy resin (Lin et al., 2021). After sintering at 610 °C, the scaffold achieved a porosity of 64.4% and compressive strength of 20.05 MPa. In vivo studies in rat femoral condyle models confirmed enhanced cancellous bone regeneration and controlled Mg degradation via CT/X-ray analysis. In 2024, Lai et al. engineered a multifunctional MgO₂/poly (lactic-co-mannitol glycolic acid) scaffold for sequential Mg²⁺ and reactive oxygen species release in Figure 1f (Li et al., 2024). This porous system portraited in Figure 1g synergistically prevented tumor recurrence via H2O2induced apoptosis/ferroptosis and M1 macrophage polarization. It also inhibited bacterial infection and promoted bone repair via Mg^{2+} -mediated Wnt3a/GSK-3 β / β -catenin pathway activation and M2 macrophage polarization as schemed in Figure 1h.

In terms of Mg-containing ceramic-polymer composites, they have also emerged as a cutting-edge material in this field. For instance, in Figure 1i Karim et al. developed amorphous magnesium phosphate (AMP)-polylactic acid (PLA) composites via melt blending. AMP-PLA scaffolds exhibited superior preosteoblast adhesion, proliferation and accelerated degradation

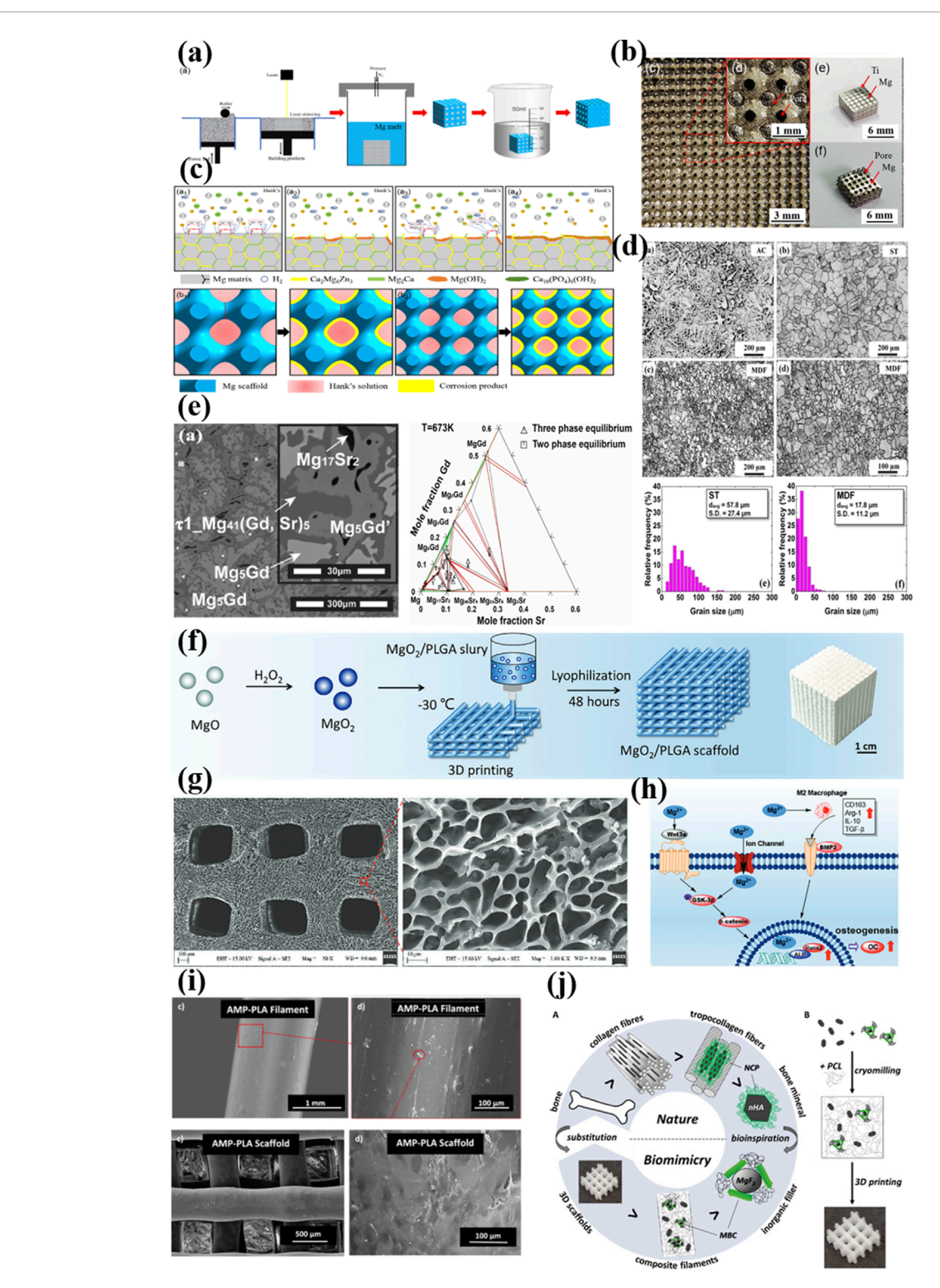


FIGURE 1

(a) Flowchart of the preparation of Mg alloy scaffolds ZMX101 alloy scaffold (Yu et al., 2024); Copyright 2024, John Wiley and Sons (b) The intermediate of Ti and Ti-Mg alloy scaffold (Yu et al., 2024); Copyright 2024, John Wiley and Sons (c) Corrosion mechanism of the ZMX101 alloy scaffolds (Yu et al., 2024); Copyright 2024, John Wiley and Sons (d) optical microstructures of the Mg-ZZn-0.2Ag alloy in AC (as-cast), ST (Solution treated) and MDF (multi-directional forging) states (Asadollahi et al., 2024); Copyright 2024, Springer Nature (e) BSE-SEM image and the isothermal sections of the Mg-rich Mg-Gd-Sr system at 673K (Long et al., 2023); Copyright 2023, Elsevier (f, g) Preparation and characterization of MgO₂ nanoparticles and MgO₂/PLGA scaffolds (Li et al., 2024); Copyright 2023, John Wiley and Sons (h) Schematic diagram of potential pro-osteogenesis mechanism of MgO₂/PLGA scaffolds (Li et al., 2024); Copyright 2023, John Wiley and Sons (i) 3D printed AMP-PLA scaffold and MC3T3 adhesion after a 7 day culture (Elhattab et al., 2021); Copyright 2021, American Chemical Society (j) compatibilized MgF₂ (cMgF₂) and nHA blended in mPCL by gentle cryomilling and fabricated into porous 3D scaffolds using a melt extrusion-based additive manufacturing system (Bas et al., 2019). Copyright 2021, American Chemical Society.

compared to pure PLA (Elhattab et al., 2021). Salil et al. fabricated poly(ϵ -caprolactone)-calcium magnesium phosphate scaffolds mimicking natural bone matrix texture, porosity, and chemistry. The NIH/3T3 fibroblast assays revealed >100% viable cells by day 3 versus controls (Parupelli et al., 2023). And bioinspired from bone non-collagenous proteins, Hutmacher et al. synthesized a ternary composite of medical-grade PCL (mPCL), nanohydroxyapatite(nHA) and compatibilized MgF $_2$ nanoparticles as depicted in Figure 1j (Bas et al., 2019). MgF $_2$ nanoparticles were functionalized with peptide-PEG conjugates to biomimicking the bone non-collagenous proteins. The mPCL/nHA/cMgF $_2$ scaffolds demonstrated impressively enhanced mechanical properties, osteogenic differentiation, and mineralization *in vitro*.

3 Classification of 3D-printing technique for Mg-containing biomedical materials

The history of 3D printing in biomedical applications dates back to the late 1980s, shortly after the invention of stereolithography by Charles Hull in 1986 (Huang et al., 2020). It witnessed great developments in the past 20 years, and now it could be broadly classified into material extrusion, vat photopolymerization, powder bed fusion, binder jetting, material jetting, and direct energy deposition categorized by material deposition method. Considering the character of magnesium, concurrently Selective Laser Melting (SLM), Wire Arc Additive Manufacturing (WAAM) and Binder Jet (BJAM) methods have been widely used in the additive manufacturing of Mg-containing alloys for biomedical application.

3.1 SLM technique

The principle of SLM molding is based on additive manufacturing, where the metal powder particles are selectively melted layer by layer to actually form a solid, dense metal part using a high-powered laser (Sing et al., 2016; Wu et al., 2021; Zhang and Attar, 2016; Murr et al., 2009; Vandenbroucke and Kruth, 2007). As depict in Figure 2a, first a thin layer of metal powder is evenly spread across a build platform. Second a highpower fiber laser selectively scans and fully melts the powder in areas defined by the 3D model current layer. This creates a fully dense metal structure. After each layer is melted and solidified, the build platform lowers slightly, and a new layer of powder is spread on top. The process repeats until the entire part is formed. Finally, the build chamber cools and the solidified part is then removed from the workbench. Compared with Selective Laser Sintering, the whole SLM has been processed under inert atmosphere to avoid the oxidation of metal powder under elevated temperature. SLM produces fully dense, high-strength and high accuracy metal parts and therefore have great advantages in printing magnesium-containing biomedical implants.

Research on SLM of Mg-containing metals could date back to the mid-2000s (Ng C. C. et al., 2011; Ng ChiChung et al., 2011). Early investigations primarily focused on understanding the feasibility of processing magnesium and its alloys using SLM, given their relatively low melting points and high chemical reactivity,

particularly in the presence of oxygen. These characteristics pose significant challenges for the actual feasibility.

To face the above-mentioned challenges, a thorough understanding of the thermodynamics and kinetics involved in the SLM process have been carried out in the last 10 years. In 2024, Liu et al. systematically investigated the effects of process parameters, structural design, and post-treatment on ZK60 magnesium alloy scaffolds fabricated by SLM (Liu Hao. et al., 2024). By employing three different structural models of Gyroid, Diamond, and Dodecahedral (Figure 2b), the authors achieved refined microstructures and improved mechanical and corrosion properties. Under optimized printing parameters, the scaffolds reached a relative density above 97%. After electrolytic polishing, the Gyroid model exhibited the largest surface area and smooth transitions, while the Dodecahedral model demonstrated the best mechanical performance, with a yield strength of 24 MPa and an elastic modulus of 425 MPa. In addition, the corrosion rate was significantly reduced from 5.67 mm/year to 1.34 mm/year for Gyroid model, as the designed larger exposure area in Hank's solution results in a denser accumulation of Ca/P corrosion products on the surface (Figure 2c). The interaction between the laser and different metal powder in SLM have also been tremendously investigated. Xie et al. explored the influence of zinc content on powder characteristics, porosity, microstructure, and corrosion behavior in SLM-processed Mg_xZn_{0.2}Mn alloys (Bian et al., 2024). Increasing Zn content led to larger powder and pore sizes, as well as reduced corrosion resistance due to more severe localized corrosion. Hu et al. examined the impact of T4 solution treatment on the microstructure and corrosion behavior of SLM-fabricated AZ91D alloys (Figures 2f,g) (Xie et al., 2023). The T4 treatment could dissolve β -Mg₁₇Al₁₂ phases to improve grain uniformity (Figure 2f) and therefore significantly enhanced corrosion resistance by 70% and reduced hydrogen evolution rate by 57%. Besides the yield strength remained as high as 181 MPa. Hendea et al. combined mechanical alloying (MA) with SLM to produce Mg-10Zn-0.8Ca-0.5Zr biodegradable implants with customized geometries (Hu et al., 2023). The MA process yielded spherical, homogenous powders suitable for SLM. And the printed samples exhibited low porosity of less than 1% and mechanical properties comparable to human bone. Corrosion behavior was also comparable to commercial ZK60 alloys. AlMangour et al. studied the feasibility of fabricating pure magnesium via SLM using a combination of experimental and fullscale simulation approaches (Hendea et al., 2023). They identified optimal densification windows between 80 and 140 J/mm³ and revealed twin-structured microstructures associated with rapid solidification. Their work provided theoretical insights into the densification and thermal behavior of magnesium under different energy densities.

The understanding of SLMed Mg-containing material has also been deepened. Recent studies by Bian et al. reported an unusual "bulk corrosion" mode in SLM-processed AZ91D magnesium alloys (Figures 2d,e) (AlMangour et al., 2023). This corrosion mechanism was attributed to the highly reactive microstructure introduced by the SLM process, including microstructural defects, dislocation density and localized strain. It resulted in corrosion rates two orders of magnitude higher than conventional counterparts. Highresolution CT scans and corrosion tests demonstrated that surface

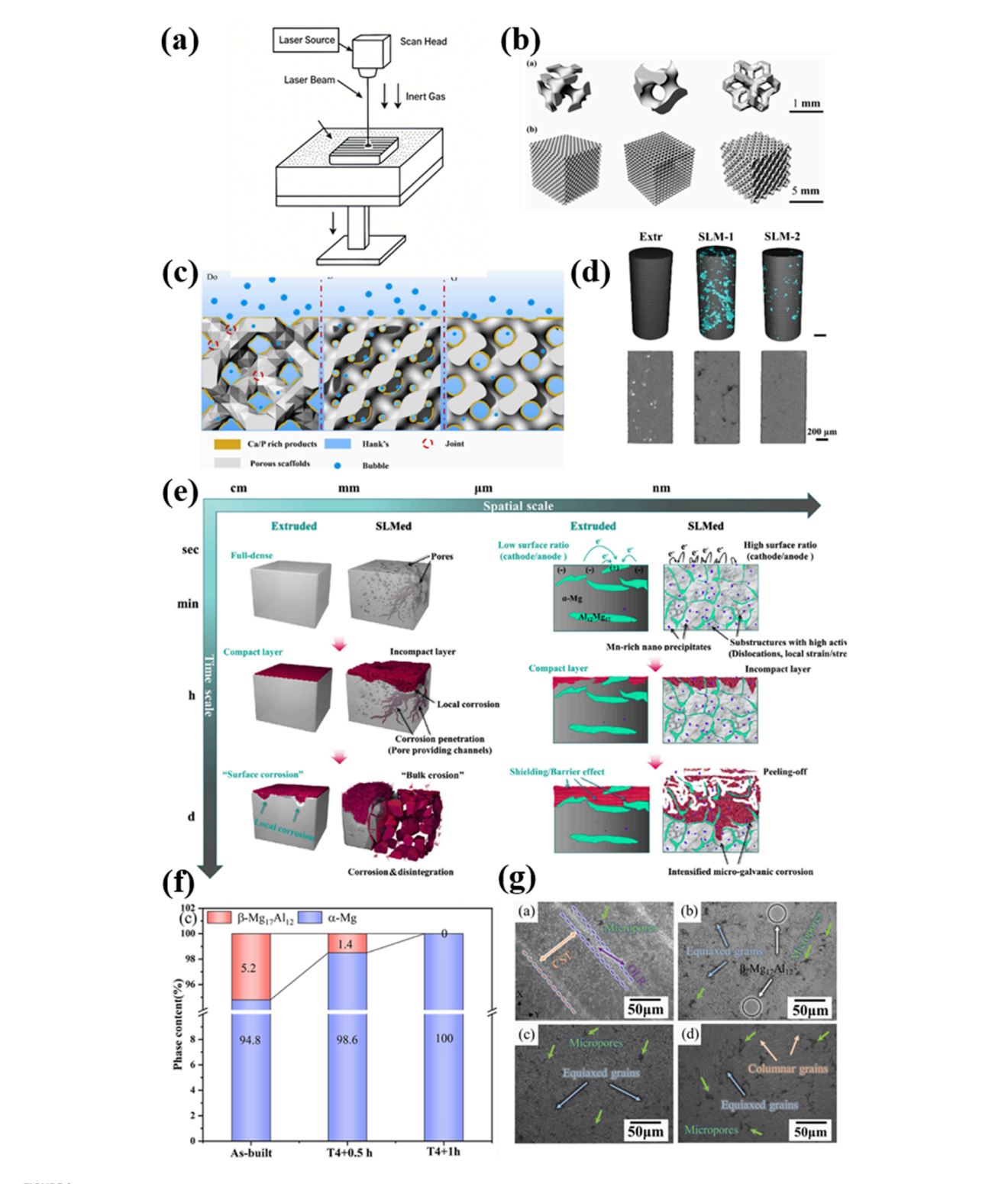


FIGURE 2 (a) The illustration of SLM printing; (b) diamond (D), gyroid (G), and Dodecahedron (Do) model of the three different AM Mg scaffolds (Liu et al., 2024b); Copyright 2024, Elsevier (c) Corrosion mechanism diagrams for G, D, and Do models (Liu et al., 2024b); Copyright 2024, Elsevier (d) 3D reconstructions under HR μ -CT. Defects were rendered with cyan (AlMangour et al., 2023); Copyright 2024, Elsevier (e) The spatiotemporal bulk erosion" mode compared with the "surface corrosion" mode (AlMangour et al., 2023); Copyright 2024, Elsevier (f) Phases content of as-built and T4 treatment (Xie et al., 2023) Copyright 2023, Elsevier.

flaws initiated rapid penetration, leading to material disintegration, significant cytotoxicity, and adverse bone reactions *in vivo*.

In terms of application scenarios, recent investigations have attempted to extend SLM technique for surface modification. In 2021, Yao et al. applied SLM for surface modification of Mg-Ca and Mg-Zn-Ca alloys, achieving improved microhardness and reduced corrosion rates from 2.1 to 1.0 mm/year. These enhancements were attributed to laser-induced grain refinement as well as impurity suppression. In another study, Yao et al. fabricated a Febased amorphous Fe₄₈Cr₁₅Mo₁₄B₆C₆ (MG) layer on pure Mg via SLM (Yao et al., 2022). The resulting Mg/MG hybrid composite exhibited dramatically improved mechanical strength. The hardness increased from 0.46 GPa to 14.3 GPa and the elastic modulus increased from 44 GPa to 202 GPa. The corrosion resistance was also reduced from 0.89 to 0.11 mm/year, alongside excellent cell adhesion and low cytotoxicity. And recently Cao et al. managed to fabricate porous Zn-1 Mg-0.1Sr scaffolds (a Mg-containing Zn alloy) using SLM, which exhibited promising potential for bone implant applications (Cao et al., 2024). The scaffolds showed a compressive strength of 33.71 \pm 2.51 MPa, a yield strength of 27.88 \pm 1.58 MPa, and an elastic modulus of 2.3 \pm 0.8 GPa. In vitro degradation tests revealed a corrosion rate of 0.36 ± 0.01 mm/year after 14 days. Extracts at 10% and 20% concentrations enhanced MC3T3-E1 preosteoblast activity with no observed cytotoxicity. However, the impact of high-concentration extracts and degradation byproducts requires further in vivo evaluation.

3.2 WAAM technique

Wire Arc Additive Manufacturing (WAAM) is a form of Directed Energy Deposition that utilizes an electric arc as the heat source and metal wire as the feedstock to fabricate large-scale metallic components layer by layer (Javadi et al., 2019; Zuo et al., 2022). According to Figures 3a,b, (Yi et al., 2022; Han et al., 2018), the principle behind WAAM involves melting the wire using a welding arc and depositing the molten material onto a substrate, where it solidifies to form the desired geometry. Typical procedures are as follows: first a metal wire feedstock is loaded into a wire feeding system. And metal-based substrate is thoroughly cleaned and fixed onto the build platform. An inert shielding gas is continuously supplied to the melt pool to prevent metal oxidation and contamination during process. Second, the electric arc is initiated between the wire electrode and the substrate. The wire melts in the arc heat and deposits onto the substrate, forming a weld bead. Third, the torch follows the programmed toolpath to deposit material layer by layer. Each layer solidifies before the next is added. Inter-layer temperature may be controlled to reduce residual stresses and improve bonding. Finally, the manufactured part is subjected to surface treatment to ensure dimensional accuracy and quality compliance.

Compared to other additive manufacturing techniques like SLS and SLM, which use powdered materials and high-energy lasers to fuse particles within a powder bed, WAAM offers significantly higher deposition rates and is more cost-effective for producing large metal parts. However, WAAM typically yields lower dimensional accuracy and surface quality, requiring post-processing, while SLM and SLS can achieve finer resolutions and are better suited for intricate geometries.

As an emerging technique in additive manufacturing, WAAM processed Mg-containing materials are relatively in the early stage of understanding the feasibility and advantages in biomedical field. In 2018, Han et al. investigated WAAM of AZ91D magnesium alloy and found that the resulting samples exhibited dense, crack-free microstructures composed of a hexagonal close-packed Mg matrix and finely dispersed Al₅Mg₁₁Zn₄ precipitates as depicted in Figure 3c (Han et al., 2018). Electrochemical impedance spectroscopy revealed improved corrosion resistance compared to cast AZ91D, indicating the potential for biomedical uses. Very recently, Cai et al. explored Gas Tungsten Arc-based WAAM (GTA-WAAM) for AZ91D fabrication (Figure 3d) (Cai et al., 2024). Their study presented the alternation of coarsen and fine grain zones and the dynamic dissolution and re-precipitation of β-Mg₁₇Al₁₂ and Al₈Mn₅ during thermal cycling. The resulting components had isotropic mechanical properties, with a tensile strength of 243.6 MPa and elongation capability of 11.7%. Manjhi et al. employed Cold Metal Transfer (CMT)-based WAAM to manufacture AZ31 alloy thin walls (Figure 3e) (Manjhi et al., 2023). The microstructure consisted of equiaxed grains with varying sizes along the build height. The precipitates β -Mg₁₇Al₁₂ and η -Al₈Mn₅ enhanced both mechanical strength and corrosion resistance in Hank's balanced salt solution, outperforming wrought AZ31 in corrosion performance (Figure 3f). And Gneiger et al. developed a high strength AEX11 magnesium alloy (Mg-Al-Zn-Ca-RE) tailored for WAAM, showing superior performance compared to commercial AZ61, especially after T6 heat treatment (Gneiger et al., 2020). The enhanced properties were attributed to the formation of Mg₁₇Al₁₂ and Al-RE strengthening phases and refined grain structures with low porosity.

In perspective of process optimization, several progresses have also been accomplished. For instance, Ying et al. studied the effects of process parameters on WAAM of AZ61 alloy. Under optimal conditions of current, voltage and wire feed rate, the alloy exhibited refined equiaxed grains, low porosity, and excellent mechanical properties (UTS of 260 \pm 14 MPa, elongation of 16% \pm 3%) (Ying et al., 2022). And Yang et al. optimized deposition parameters for NZ30K alloy (Mg-Nd-Zn-Zr) in WAAM (Yang et al., 2025). Their findings emphasized the sensitivity of weld bead quality to current and travel speed, identifying 100–120 A and 2–3 mm/s as the optimal range to avoid macro/micro defects and achieve good metallurgical bonding.

3.3 Binder jet technique

Binder Jet is a powder bed-based additive manufacturing process where a liquid binder is selectively deposited onto a bed of metal powder to form a solid part layer-by-layer. For Mg-containing alloys, the process begins with the uniform spreading of a thin layer of alloy powder over the build platform. An inkjet printhead then selectively deposits a binder onto regions defined by the digital cross-section of the 3D model. This creates a "green" part with low mechanical strength.

After each layer is completed, the powder bed is lowered, and a new powder layer is spread. This process is repeated until the entire part is formed. Once printing is complete, the green part is carefully removed from the surrounding unbound powder and subjected to post-processing steps, typically including curing, de-binding, and

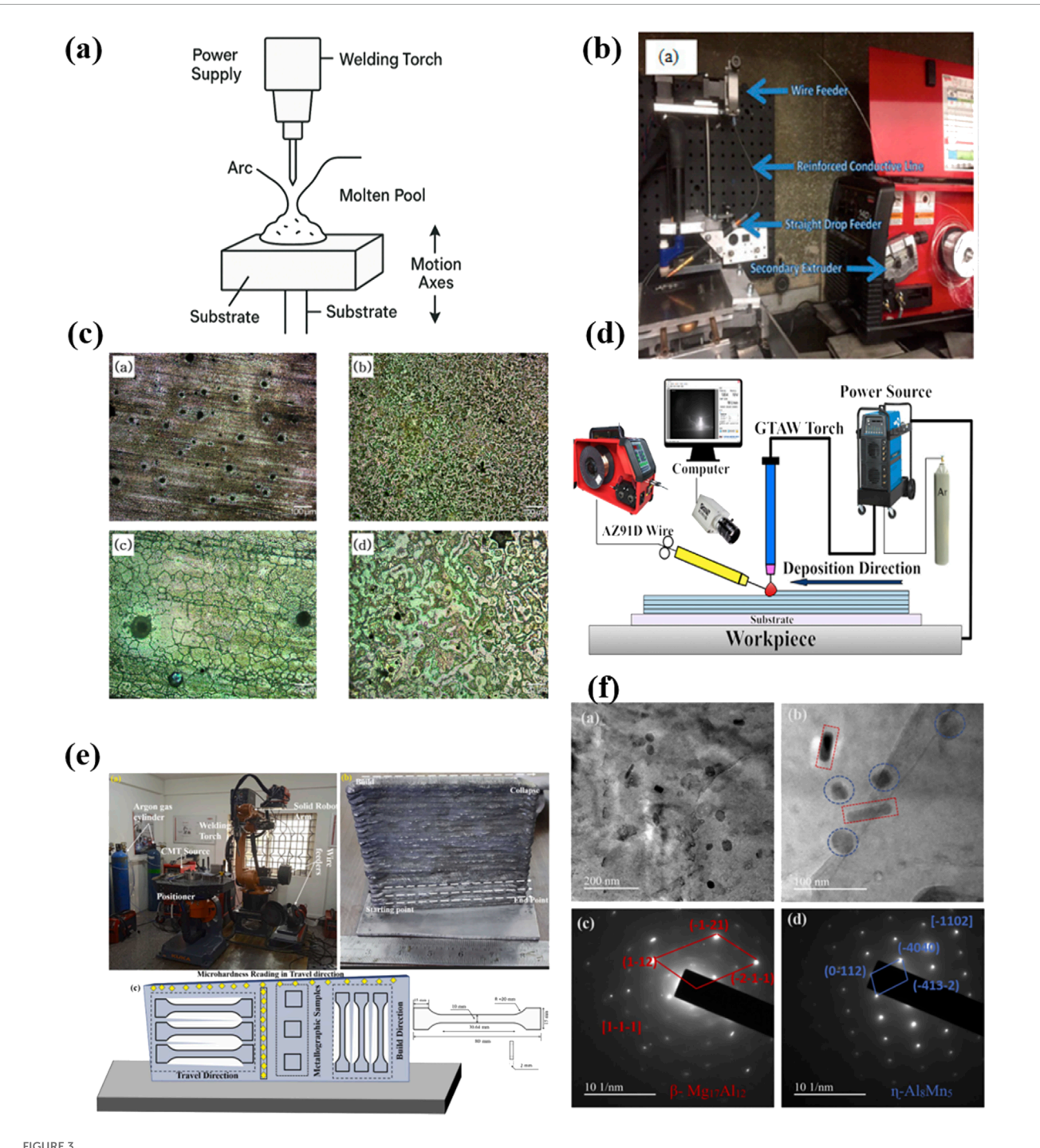


FIGURE 3
(a) The illustration of WAAM printing; (b) an overall system for WAAM (Han et al., 2018); Copyright 2018, Mdpi (c) After corrosion microstructure of AZ91D produced by WAAM and casting (Han et al., 2018): (a,c) AZ91D casted; (b,d) AZ91D WAAM; Copyright 2018, Mdpi (d) GTA-WAAM system and the fabricated component (Cai et al., 2024); Copyright 2024, KeAi (e) CMT-WAAM process experimental setup and AZ31 Mg alloy deposited thin wall with samples used for metallurgical, mechanical, and corrosion test (Manjhi et al., 2023); Copyright 2023, Elsevier (f) TEM Analysis (a-b) secondary phase particles in the α-Mg matrix and (c-d) selected area electron diffraction (SAED) patterns of WAAMed AZ31 (Manjhi et al., 2023). Copyright 2023, Elsevier.

high-temperature sintering under controlled atmospheres to densify the structure and achieve desired mechanical properties (Figure 4a).

In recent years, Binder Jet Additive Manufacturing (BJAM) has emerged as a promising, scalable, and geometry-friendly technique for processing Mg alloys at low-temperatures. Currently, ongoing research has focused on powder preparation, sintering

enhancement, composite reinforcement, pore architecture control, and bio-surface modification to improve densification, mechanical strength, and biocompatibility of the printed components. For instance, Zhao et al. successfully fabricated high-density AZ91D-based composites via BJAM by adding SiC particles (Zhao et al., 2025). The addition of SiC effectively disrupted the surface oxide

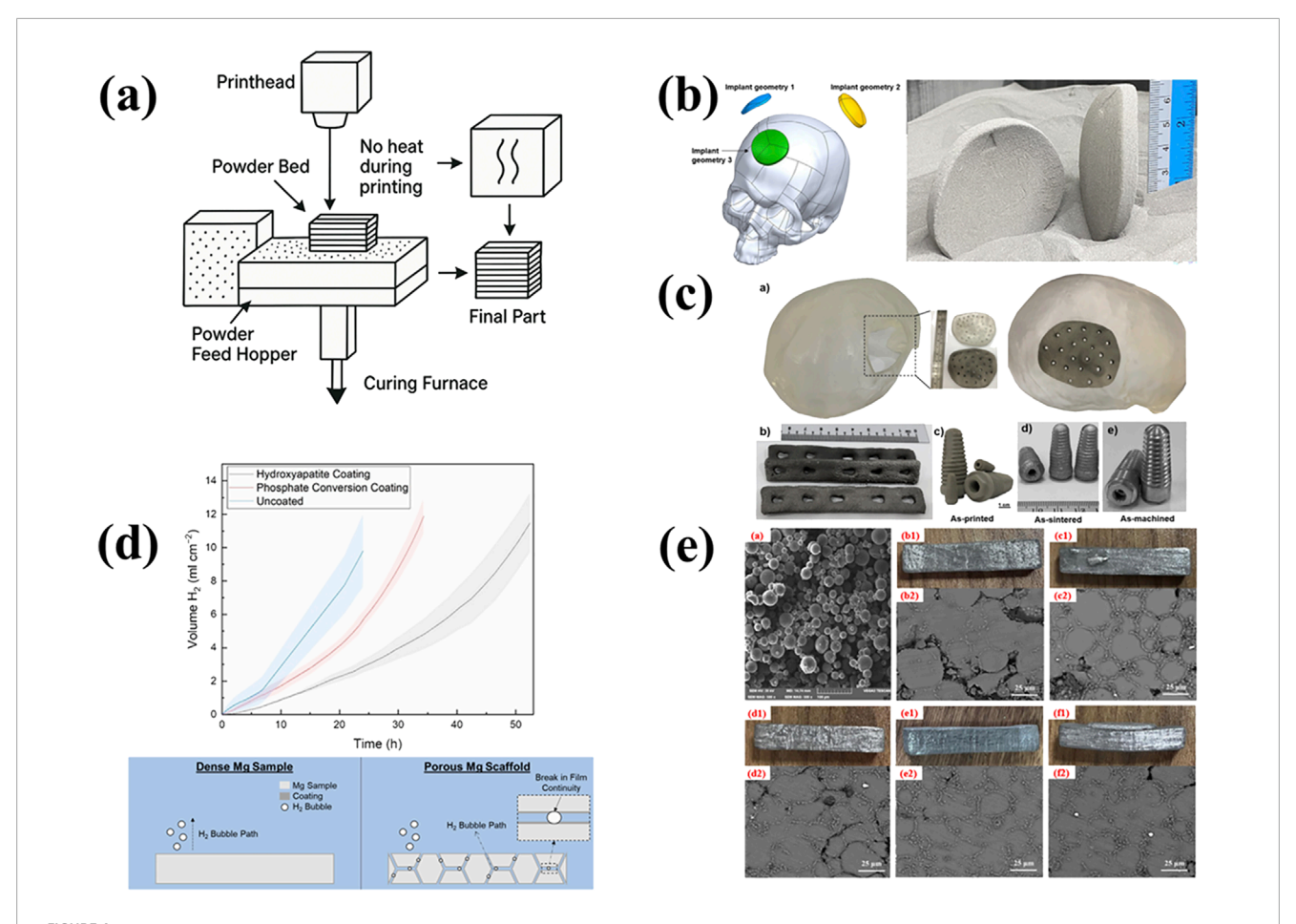


FIGURE 4
(a) The illustration of BJAM printing; (b) Binder-jet printed and sintered Mg-Zn-Zr parts for biomedical applications (Salehi et al., 2025); Copyright 2025, Elsevier (c) Binder jet printed spherical cap-shaped Mg implants inspired by the shape of human partial skull, in the green condition (Salehi et al., 2024); Copyright 2024, KeAi (d) Hydrogen evolution comparison between uncoated, hydroxyapatite-coated and phosphoric on coated porous Mg-Zn-Zr scaffolds with phosphate conversion coating forming process (Kuah et al., 2022); Copyright 2022, Mdpi (e) Microscopic morphology of the green body; and the macroscopic morphologies and microstructures of the sintered bodies under different stepwise sintering processes (Zhang et al., 2025). Copyright 2025, Elsevier.

layer on Mg particles and enhanced liquid-phase infiltration. It resulted in a sintered density of 97.02% and a compressive strength of 235 MPa, demonstrating the synergistic effect on sintering densification and mechanical performance. In Figure 4b, Salehi et al. explored the biomedical potential of BJAM-processed Mg-Zn-Zr scaffolds that mimic the cortical bone structure, achieving a tensile strength of 130 MPa and compressive strength of 349 MPa with excellent cytocompatibility (Salehi et al., 2025). They also proposed a hybrid manufacturing workflow integrating BJAM with automated dry machining to enable digital manufacturing of patient-specific implants as presented in Figure 4c (Salehi et al., 2024). The resulting surface roughness of 1.05–1.28 μ m satisfied clinical implant standards.

To address the challenge posed by native MgO layers during sintering, Salehi further introduced calcium-containing ceramic nanoparticles as sintering aids (Salehi et al., 2023b). These nanoparticles would react with MgO to form CaO, reducing oxide thickness and increasing relative density to 93.5%, alongside improvements in elongation and tensile properties. Kuah et al. applied hydroxyapatite (HA) and phosphate conversion coatings

to porous Mg-Zn-Zr scaffolds (Kuah et al., 2022). These coatings significantly reduced the corrosion rates by up to 4.8-fold compared to uncoated dense samples (Figure 4d). However, hydrogen entrapment within pore channels still limited the overall protective effect.

Furthermore, the fabrication steps have also been optimized. In Figure 4e, Zhang et al. investigated the effects of stepwise sintering protocols on the microstructure and properties of BJAM-fabricated AZ91D parts (Zhang et al., 2025). The optimal strategy yielded a relative density of 91.77%, compressive strength of 202.33 MPa, and tensile strength of 89.45 MPa, remarkedly higher than those obtained via traditional two-step sintering.

3.4 Inkjet printing (3D-gel printing)

To address the issue of printing Mg containing composite material, in 2016 Ren et al. proposed a modified direct inkjet printing called 3D-gel printing, which utilizes radical polymerization of organic monomer to hold the composite material

to form the green part of the scaffold (Ren et al., 2016). As depicted in Figure 5a, a typical 3DGP process is composed of four main steps, which are premixing solution, slurry preparation, initiator addition and printing. Compared with custom 3D printing technique, the 3D-gel printing extends the printable materials further to ceramic, metal and their composites (Figure 5b). And both cost and energy consumption are reduced as high-energy beam and inert gas atmosphere are no longer needed in the process.

In 2020, Shao et al. fabricated porous Mg_xCa_{3,x}(PO₄)₂ composite scaffolds using 3DGP combined with liquid-phase precipitation of precursor powders (Figure 5c) (Shao et al., 2020). The research systematically investigated the effects of different Mg²⁺ doping levels on scaffold properties. Results showed that increasing Mg²⁺ content reduced powder particle size with enhanced sintering behavior. The as-fabricated scaffolds presented decreased porosity and improved compressive strength of a maximum of 1.89 \pm 0.21 MPa. Degradation studies in PBS revealed that Mg doping initially promoted weight gain due to apatite precipitation but slowed the degradation over time. While the mechanical strength remains best suited for cancellous bone repair, the scaffolds exhibited good bioactivity and biodegradability. Notably, the 3DGP technique offered significant advantages including precise control over scaffold geometry, interconnected porous structure, material versatility, cost-effective processing and customization potential.

In 2023, Lin et al. made the first attempt to fabricate Mg-containing scaffold using the 3DGP (Figure 5a) (Lin et al., 2023). The process involved preparing a printable slurry of Mg and Zn powders with an optimal solid content of 60%, followed by extrusion-based printing and sintering. Compared to laser-based additive manufacturing, 3DGP avoids flammability issues with Mg powder and reduces oxidation risks. And the shrinkage was <5% after sintering, maintaining scaffold geometry. In addition, they found that adding a small amount of 10 wt% Zn significantly improved mechanical strength up to 13.03 MPa and corrosion resistance, making the 0.9Mg–0.1Zn composition most suitable for bone engineering applications.

3.5 Extrusion-based 3D printing

Extrusion-Based 3D Printing is another additive manufacturing technique for Mg containing composite material for fabricating tissue engineering scaffolds. In this process, a thermoplastic polymer such as polycaprolactone (PCL) is heated above its melting point and extruded with composite materials through a fine nozzle to form continuous filaments. These filaments are deposited layer by layer according to a computer-aided design model to create 3D structures with controlled geometry, porosity, and architecture.

Abdalla Abdal-hay presented a novel approach to fabricating bioactive, biodegradable scaffolds for bone regeneration in Figure 5d (Abdal-hay et al., 2020). Using extrusion-based 3D printing, PCL was blended with 5% and 20% weight of magnesium hydroxide (MH) nanoparticles (<50 nm) and extruded at 95 °C through precision needles to produce scaffolds with six orthogonal layers. The printed PCL/MH scaffolds demonstrated interconnected porosity, enhanced tensile modulus and a controlled degradation profile over 150 days. *In vitro*, the scaffolds supported superior

osteoblast adhesion, proliferation, and differentiation via ALP and RUNX2 expression compared to PCL-only controls as depicted in Figure 5e. The study highlights the potential of MH as a biocompatible filler that tailors both mechanical and biological properties, offering a promising 3D printable solution for bone tissue engineering applications.

3.6 Fiber deposition-based 3D printing technique

Fiber deposition-based 3D printing is an emerging additive manufacturing technique that integrates fiber reinforcement into a thermoplastic matrix with layer-by-layer deposition. This technique enhances the mechanical performance of printed parts, making it particularly attractive for load-bearing biomedical applications such as orthopedic implants and prosthetics.

Fu et al. managed the magnesium phosphate-zinc silicate bioceramic scaffold with three-dimensional macro-porous structure by this technique (Fu et al., 2025). The incorporation of zinc silicate could lower the scaffolds porosity to increase the scaffold compression strength. And this scaffold gradually degraded in aqueous environment with the simultaneous release of Zn and Si ions, which further enhance the cell proliferation and osteogenic differentiation.

To summarize the differences of above-mentioned 3D printing techniques for Mg-containing biomaterials, the key processing parameters, advantages and current limitations have been listed in Table 1.

4 Evaluation of 3D printing Mg-containing biomedical materials

3D-printing magnesium-containing biomedical materials have to meet a series of stringent performance requirements before actual clinical applications. These requirements encompass biocompatibility, mechanical properties, degradability, corrosion resistance, as well as other indicators related to safety and efficacy (Liang et al., 2023; Hu et al., 2023; Zhai et al., 2023).

4.1 Biocompatibility evaluation

Mg fabricated via SLM exhibited promising biocompatibility attributes for temporary implants, but notable caveats still remain. The degradation products, mainly Mg²⁺ ions were generally nontoxic and participate in natural metabolic pathways promoting osteogenesis and bone healing. They were demonstrated by multiple *in vitro* and *in vivo* studies (Liu Hao. et al., 2024; Cao et al., 2024). However, adverse reactions were observed in certain SLM fabricated Mg alloys. This adverse effect could lead to rapid material disintegration, local alkalinity, hydrogen gas accumulation, and inflammatory responses (AlMangour et al., 2023). While most SLM fabricated Mg implants did not provoke immune rejection or allergic responses, we note that fast degradation can still cause mechanical failure and local tissue damage before healing completes (Bian et al., 2024; Xie et al., 2023). Moreover,

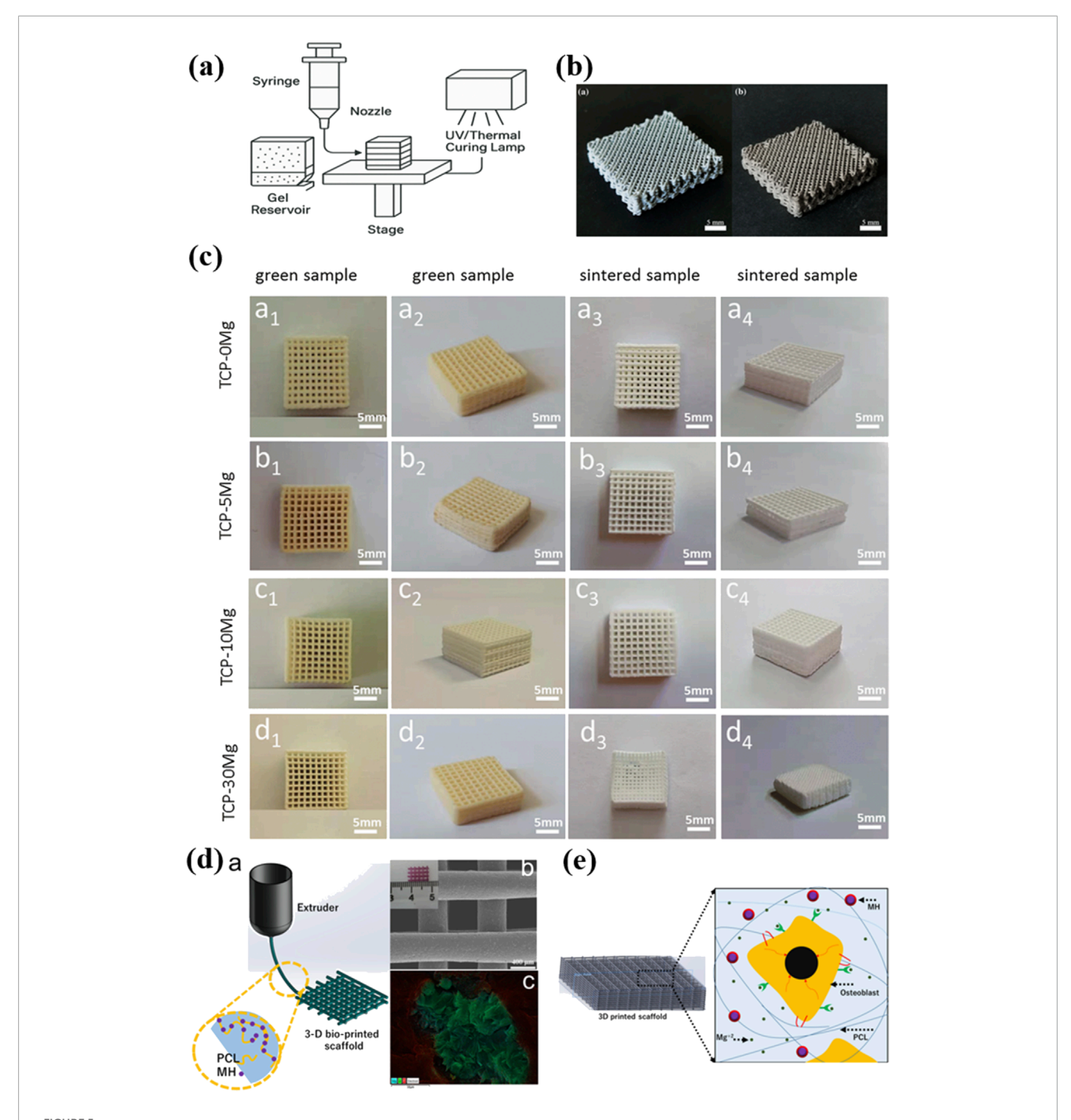


FIGURE 5 (a) The illustration of 3DGP printing; (b) Porous Mg-xZn scaffolds prepared by the 3DGP process (Ren et al., 2016); Copyright 2016, Elsevier (c) The macro view of $Mg_xCa_{3-x}(PO_4)_2$ porous scaffolds printed by 3DGP (Shao et al., 2020); Copyright 2020, Springer Nature (d) Schematic diagram of the additive manufacturing fabrication process and SEM image of the fabricated 3D PCL/MH composite scaffold (Abdal-hay et al., 2020); Copyright 2020, Elsevier (e) Schematic diagram of the 3D microenvironment created by the PCL/MH nanocomposite scaffold which showing beneficial effect on cellular behavior (Abdal-hay et al., 2020). Copyright 2020, Elsevier.

surface modifications or alloying helped fine-tune degradation rates and microstructural homogeneity, improving both mechanical and biological performance (Yao et al., 2022; Yao et al., 2021). However, excessive ion release or secondary phase formation could still lead to localized toxicity and galvanic corrosion (Yao et al., 2021).

WAAM Studies on AZ31 and AZ61 alloys confirmed that with proper parameter tuning, WAAM could produce equiaxed grains and uniform microstructures, minimizing stress concentrations that might trigger immune rejection or inflammation (Manjhi et al., 2023; Ying et al., 2022). By extra ultrasonic vibration, it could significantly reduce grain size and improve corrosion resistance,

TABLE 1 The comparison of different 3D printing techniques.

Technique	Key process parameters	Advantages	Current limitations
Selective Laser Melting (SLM)	laser power, scan speed, hatch spacing, layer thickness, inert gas atmosphere	high precision, fully dense parts, complex porous structures, tunable microstructure	risk of oxidation and flammability, process sensitivity, bulk corrosion issues, expensive setup
Wire Arc Additive Manufacturing (WAAM)	arc current and voltage, wire feed rate, travel speed, shielding gas flow, inter-layer temperature	high deposition rate, cost-effective for large components, scalable	lower accuracy and surface quality, risk of coarse grains, requires post-processing
Binder Jet Additive Manufacturing (BJAM)	powder layer thickness, binder saturation level, curing and sintering temperature, powder characteristics	low temperature process, good design freedom, near-room temperature operation	low green part strength, challenges in densification, rapid degradation due to porosity
3D Gel Printing (3DGP)	slurry composition, initiator concentration, extrusion speed, curing and sintering profile	low oxidation risk, cost-effective, suitable for composites, shape fidelity	limited mechanical strength, shrinkage after sintering, limited for non-load-bearing
Extrusion-Based 3D Printing	extrusion temperature, nozzle diameter, printing speed, polymer/ceramic/Mg filler ratio	simple process, material versatility, biocompatible composites, porous scaffolds	lower mechanical strength than metals, slow printing speed, limited load-bearing use
Fiber Deposition-Based 3D Printing	deposition temperature, fiber orientation, feed rate, matrix–fiber compatibility	enhanced mechanical strength with fiber reinforcement, suitable for load-bearing implants	complex process control, compatibility issues, limited research in biomedical field

thereby lowering the risk of harmful by-products and promoting better tissue integration (Chen et al., 2025). However, high heat input in WAAM could induce coarse grains or columnar structures in some alloys, potentially leading to uneven degradation and compromised healing if not properly controlled.

From the biocompatibility standpoint, BJAM allows for high design freedom and near room temperature printing, reducing risks associated with oxidation or thermal decomposition. However, low initial density of green parts and the formation of MgO surface layers impede densification during sintering, thus affecting mechanical performance and biocompatibility. Therefore, the rapid degradation exacerbated by the high surface area of porous structures produced through BJAM would lead to excessive hydrogen evolution, which may form gas pockets and hinder tissue integration (Kuah et al., 2022).

For 3DGP, the degradation products of the printed Mg-containing scaffolds would primarily be consisted of magnesium hydroxide and phosphate-related compounds, which were found to be non-toxic and could be safely metabolized or excreted by the human body. Taking this advantage, the Mg-Ca-P scaffolds fabricated using 3DGP showed gradual degradation behavior in simulated body fluid, with pH stabilization over time, indicating buffered and biocompatible degradation without excessive alkalization (Ren et al., 2016). But more vitro and vivo experiments need to be done before clinical application.

4.2 Mechanical evaluation

The customized Mg-containing biomedical materials must also possess mechanical properties comparable to those of human bone to ensure their ability to bear loads and support normal skeletal function. In terms of strength and hardness, the yield strength, tensile strength, and hardness of the material should be close

to or slightly lower than those of natural bone to prevent stress shielding effects and maintain physiological load transfer. From the perspective of flexural deformation, the elastic modulus of Mg-containing materials should approximate that of cortical bone, typically ranging from 10 to 30 GPa. An excessively high modulus may lead to stress concentration and uneven load distribution, while a modulus that is too low may result in insufficient mechanical support. Furthermore, adequate toughness and ductility are essential to prevent brittle fracture and sudden failure under mechanical stress. We note that the composition of the alloy and the structural design of the scaffold are in strong relationship to the mechanical properties, the characteristic of different 3D printing technique (e.g. composition, temperature, porosity) do exhibit distinct application trajectories regarding to the mechanical properties (Table 2).

For instance, Zn-1 Mg-0.1Sr scaffolds produced by SLM exhibited an elastic modulus of 2.3 ± 0.8 GPa and yield strength of 27.88 ± 1.58 MPa, closely resembling cancellous bone and ensuring better compatibility for low-load-bearing applications (Cao et al., 2024). Post-processing techniques such as T4 heat treatment were shown to reduce strength slightly while significantly enhancing corrosion resistance, indicating a trade-off between mechanical robustness and degradability (Xie et al., 2023). The introduction of metallic glass coatings on pure Mg not only boosted hardness from 0.46 to 14.3 GPa but also improved wear resistance without compromising structural cohesion (Yao et al., 2022).

Recent studies on WAAM-fabricated magnesium alloys reveal that their mechanical properties can be tailored to closely match those of human bone, making them promising candidates for load-bearing biomedical implants. For instance, WAAM-processed AZ91D alloys demonstrated yield strengths of around 110.5 MPa and ultimate tensile strengths up to 243.6 MPa with elongations of 11.7%. It offered a balanced combination of strength and

TABLE 2 The mechanical strength of 3D printing scaffolds with commercial and bone reference.

References	Liu et al. (2024b)	Cao et al. (2024)	Cao et al. (2024)	Cai et al. (2024)	Zhang et al. (2025)	Cai et al. (2024)	Salehi et al. (2023b)	Salehi et al. (2025)	Salehi et al. (2025)	Lin et al. (2023)	Salehi et al. (2025)	Salehi et al. (2025)
Relative density (%)	30	30	38		91.7		86.8	93.9		34.8	86.9 ± 4.2	90.6 ± 3.0
Elastic Modulus (GPa)<		2.3	0.8				21.5			0.24	11.5–32.5	9.55–17.3
Elongation (%)				11.7	69.0	3	2.1	5.7	14.0			
Ultimate tensile strength (MPa)				243.5	89.4	230	130.3	173.0	278.0		20.4–124.6	121–172.5
Tensile yield strength (MPa)		27.9	10.2	110.0		160	6.66	92.8	140.0			
Ultimate compressive strength (MPa)					202.3		349.3	407.0	354.0	14.3		
Compressive yield strength (MPa)	24	33.7	16.2						118.0		96.5 ± 35.9	167
Material and process	ZK60(SLM)	Zn-1 Mg-0.1Sr (SLM)	Porous Zn	AZ91D(WAAM)	AZ91D(BJAM-TH4)	AZ91D (ASTM standard B91-12)	Mg-Zn-Zr (BJAM)	Mg5.9Zn0.13Zr0.2Ca (BJAM)	Mg–Zn–Zr (Cast Ingot)	0.9Mg-0.1Zn(3DGP)	Cranial Bones	Femur

ductility superior to their cast counterparts (Cai et al., 2024). Similarly, CMT-based WAAM of AZ31 alloys achieved tensile strengths of 224 MPa and elongation values of approximately 23%, with improved mechanical isotropy due to equiaxed grain structures (Manjhi et al., 2023). Furthermore, the development of novel high-strength alloys such as AEX11 via WAAM has led to significant improvements, with yield strengths and tensile strengths exceeding 170 MPa and 245 MPa respectively, supported by good ductility up to 14% (Gneiger et al., 2020). These values fall within or slightly above the mechanical range of cortical bone, ensuring adequate support without inducing stress shielding.

In terms of BJAM, the recent improvements in green part densification and sintering have mitigated issues of brittleness and low ductility previously seen in early BJAM-fabricated scaffolds. Zhang et al. demonstrated that a stepwise sintering process could yield AZ91D samples with a compressive strength of 202.33 MPa, tensile strength of 89.45 MPa and density of 91.77%, which closely align with the mechanical benchmarks for cortical bone (Zhang et al., 2025). This was attributed to enhanced grain bonding and reduced porosity. Similarly, Salehi et al. reported that Mg-Zn-Zr alloys fabricated through BJAM exhibited yield strength up to 124 MPa and modulus values within 10-25 GPa, ensuring compatibility with human bone and avoiding stress shielding (Salehi et al., 2023a). Some studies also explored reinforcement strategies, such as incorporating SiC particles to increase the hardness and flexural resistance, though at the cost of some ductility (Zhao et al., 2025).

In 3DGP, Mg–Ca–P scaffolds exhibited a compressive strength of 8.1–11.6 MPa and an elastic modulus ranging from 0.3 to 0.5 GPa. These values are comparable to cancellous bone but still below those of cortical bone (Ren et al., 2016). Similarly, Mg–Zn based scaffolds reported compressive strengths up to 16.5 MPa, with mechanical integrity maintained during early-stage degradation and ensuring temporary support during bone healing. The lower elastic modulus suggests that 3DGP-fabricated scaffolds may be more suitable for non-load-bearing or moderate-load applications unless further reinforced.

4.3 Biodegradation evaluation

One significant advantage of Mg-containing metallic materials lies in their biodegradability. However, both the degradation rate and the by-products of degradation are critical factors in evaluating their performance. In general, the biodegradation of magnesium *in vivo* is primarily governed by its electrochemical corrosion in aqueous physiological environments such as body fluids, which could contain dissolved oxygen, proteins, and electrolytes. The fundamental corrosion reaction involves anodic dissolution of Mg and cathodic hydrogen evolution, which has been widely acknowledged in previous references as follows.

$$Mg \rightarrow Mg^{2+} + 2e^{-}$$

$$2H_2O + 2e^{-} \rightarrow H_2 + 2OH^{-}$$

$$Mg^{2+} + 2OH^{-} \rightarrow Mg(OH)_2$$

Initially, the generated Mg(OH)₂ film could act as a protective barrier that can slow down further corrosion. However, the protective layer could be further destabilized due to the conversion of Mg(OH)₂ into highly soluble species like follows:

$$Mg(OH)_2 + Cl^- \rightarrow MgCl_2 + 2OH^-$$

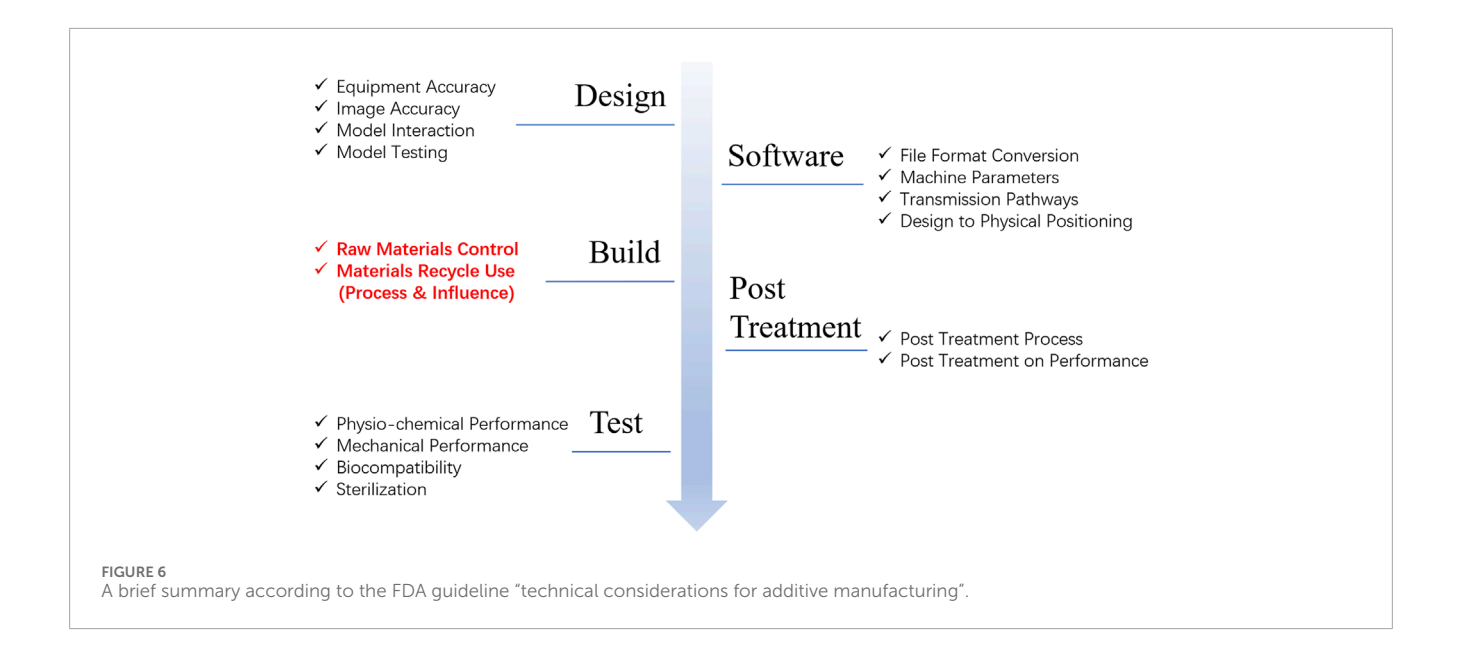
This continuous dissolution–reprecipitation cycle accelerates localized corrosion and pitting. And in porous or additively manufactured Mg structures, microstructural heterogeneities such as second phases, grain boundaries, and residual stress further intensify galvanic corrosion. Therefore, it is important to control biodegradation rate of as-prepared Mg-containing scaffolds.

Firstly, the degradation rate of Mg-containing materials should align with the healing process of bone tissue. If degradation occurs too rapidly, the implant may lose its mechanical support prematurely. Conversely if it degrades too slowly, it may result in prolonged corrosion and other complications. Ideally, the degradation period of Mg alloys should range from several months to one to 2 years, depending on the specific requirements of the implantation site. Secondly, the control of degradation to minimize hydrogen release should be considered during *in vivo* degradation. And the by-products should be non-toxic and capable of being gradually absorbed by the body.

In previous studies, SLMed ZK60 scaffolds showed a significant reduction in corrosion rate from 5.67 mm/year to 1.34 mm/year after coating treatment, highlighting the importance of surface modification in controlling degradation kinetics (Liu Hao. et al., 2024). However, some SLMed Mg alloys exhibited a bulk erosion mechanism rather than uniform surface corrosion, leading to rapid material disintegration and potential adverse tissue reactions (AlMangour et al., 2023). In contrast, the Zn-1 Mg-0.1Sr alloy scaffold demonstrated a more controlled degradation profile, with a moderate corrosion rate of 0.36 mm/year and no evidence of cytotoxic by-products, making it suitable for bone regeneration applications (Cao et al., 2024). Alloying strategies, such as incorporating Zn, Ca, Sr or rare earth elements, helped regulate the corrosion rate but also introduced risks of galvanic corrosion or potential ion-related toxicity when not optimized (Bian et al., 2024; Yao et al., 2021).

In WAAM, it enables microstructural control for tuning degradation rates. The incorporation of ultrasonic vibration during deposition could control the AZ31 corrosion rate from 0.815 to 0.200 mm/year and limiting hydrogen accumulation by promoting dense protective film formation (Chen et al., 2025). AZ61 and AZ91 alloys also exhibited decreased susceptibility to localized corrosion due to their compact grain structures and reduced intergranular defects, thereby aligning degradation more closely with tissue regeneration requirements (Ying et al., 2022; Cai et al., 2024). Moreover, advanced alloy designs, such as AEX11 and Mg-Nd-Zn-Zr compositions, introduced rare earth elements and Ca to improve corrosion stability. These elements facilitated the formation of stable, bio-inert degradation by-products while slowing down corrosion to a desirable rate (Gneiger et al., 2020; Yang et al., 2025). Although WAAM could enable microstructural control for tuning degradation rates, the in vivo validation is still necessary to ensure long-term biodegradability and safe hydrogen management in clinical.

The degradation rate of BJAM-fabricated Mg alloys was found to be highly dependent on factors such as porosity, alloy composition



and post-processing treatments. For instance, Mg-Zn-Zr scaffolds exhibited a corrosion rate of approximately 0.31 mm/year in simulated body fluid, which falls within the acceptable range for temporary orthopedic implants and supports initial phases of bone healing without causing premature loss of mechanical integrity (Zhang et al., 2025). In contrast, uncoated AZ91D samples showed significantly higher degradation rates, exceeding 0.8 mm/year, due to their high porosity and the presence of intermetallic β -Mg₁₇Al₁₂ phases that promote galvanic corrosion. Several studies applied surface modifications, such as hydroxyapatite and phosphate coatings towards reduced degradation rates by 30%-50%, bringing them closer to the desired 0.2-0.5 mm/year range (Kuah et al., 2022). For example, the Mg-Ca-P scaffolds exhibited a gradual degradation profile with weight loss rates ranging from 5.2% to 13.6% over 28 days in simulated body fluid, depending on the Ca/P ratio and sintering conditions (Shao et al., 2020).

4.4 Surface treatment

Last but not least, surface treatment of Mg-containing materials plays an increasingly important role in the development of customized medical devices. An appropriate surface roughness could enhance cell adhesion and proliferation while excessively rough surfaces may trigger undesirable tissue responses or lead to stress concentration. Therefore, surface modifications strategies such as coatings, anodization, and phosphitylation were generally adopted to improve the integration between bone tissue and the implant, thereby accelerating bone healing and enhancing osseointegration. For instance, electrolytic polishing of SLM fabricated ZK60 scaffolds led to smoother surface transitions, reducing micro-stress concentrations while maintaining interconnected porosity beneficial for tissue ingrowth (Liu Hao. et al., 2024). In contrast, unmodified SLMfabricated surfaces often presented microscale defects and residual roughness due to rapid solidification, which could exacerbate localized corrosion and adversely affect tissue compatibility (Hendea et al., 2023).

In contrast, the 3DGP technique did not offer precise, localized control of surface roughness, but it enabled bulk roughness modulation through material and sintering design. The as-printed scaffolds typically exhibit moderate to high surface roughness, with reported average roughness values ranging from 4.5 to $12 \, \mu m$ (Shao et al., 2020). Although surface roughness was demonstrated to be a key parameter in device performance, few papers have been published regarding this phenomenon.

4.5 Extra material and device evaluation for advanced manufacturing

Beyond the above-mentioned materials efficacy and safety, we notice that there are still several important evaluations that need to be done for 3D-printing biomedical materials and devices. Since customized biomedical devices are designed based on the specific needs of individual patients, they exhibit high variability and are produced in limited quantities. As a result, it is not feasible to conduct preclinical and clinical studies according to the same requirements typically applied to standardized medical devices. Therefore, the evaluation methods applicable to standardized devices are no longer fully suitable for customized medical device products.

Typically, the unique materials and devices requirements for 3D-printing technique lie in the additional material control evaluation for customized materials and devices. In 2017, the Food and Drug Administration of America guideline "technical considerations for additive manufacturing" iterated the additional material control evaluation in the fabrication of 3D-printing medical devices as labelled in red in Figure 6. The unique evaluation perspectives include control of raw material consistency and potential issues arising from material reuse and recycling during additive manufacturing. It specified that medical devices produced via additive manufacturing must describe the process of material

recycling and provide evidence demonstrating that such reuse does not adversely affect the final device. However, few papers in this review considered the recyclability of as-designed materials.

Moreover, the international medical device regulators forum also required the validation of computational models and simulation methods, along with a comparative analysis of the risk-benefit profile against conventional treatment approaches and approved alternative medical devices. Therefore, in our point of view, extra materials and devices evaluations should be established considering the unique feature of AM fabricated biomedical materials and devices.

5 Conclusion and outlook

In this review, we have comprehensively examined the current state of 3D-printing Mg-containing biomedical materials, encompassing both alloy and composites. Mg-containing alloys achieve synergistic regulation of degradation rate, mechanical properties, and biocompatibility through alloying with rare earth elements and physiological metals. Mg-containing composites further optimize degradation kinetics and multifunctionality such as anti-tumor and antibacterial through combination with polymers, ceramics or nanoparticles. These material innovations provide diverse options for 3D-printing customized bone repair implants, with the core lying in balancing the relationship among mechanical and biological activity through compositional design.

On the processing side, additive manufacturing techniques such as selective laser melting (SLM), wire arc additive manufacturing (WAAM), binder jetting (BJAM) and extrusion-based printing each offer unique advantages. These methods allow unprecedented control over scaffold geometry, porosity, and degradation behavior. But their process–microstructure-performance relationships remain highly sensitive and must be precisely optimized to ensure reliable outcomes. Collectively, these findings underline that 3D-printing Mg containing constructs have strong potential to advance customized Mg-containing implants.

Despite these promising developments, several scientific gaps and challenges remain that require further research. First, longterm in vivo degradation and safety studies are scarce and systematic investigations are needed to evaluate hydrogen release, local tissue responses and functional integration during healing. Second, material recycling and powder reuse which are critical for regulatory approval and sustainable manufacturing, remain underexplored in Mg-containing AM systems. Third, the field lacks standardized yet adaptable evaluation protocols that bridge laboratory findings with clinical requirements, especially for patient-specific devices where individualized responses must be taken considerations. Furthermore, enhancing cross-scale characterization tools that couple microstructural, mechanical, and biological performance is essential to accelerate clinical translation. Finally, interdisciplinary integration across materials science, computational modeling, and clinical practice will be crucial to optimize design pipelines, establish predictive frameworks, and validate patient-specific implants.

Addressing these challenges will pave the way for Mg-containing 3D printing to transition from experimental demonstrations to

reliable clinical solutions. With sustained collaboration across scientific and medical communities, Mg-containing 3D-printing constructs are positioned to become cornerstone technologies in next-generation orthopedics and beyond.

Author contributions

SJ: Writing – original draft, Investigation, Funding acquisition, Conceptualization. JZ: Writing – review and editing. TT: Funding acquisition, Writing – review and editing, Investigation. MY: Resources, Investigation, Writing – review and editing. CQ: Writing – review and editing, Investigation, Resources. YL: Funding acquisition, Writing – review and editing, Supervision.

Funding

The author(s) declare that financial support was received for the research and/or publication of this article. This work is granted by Natural Science Foundation of Shanghai (24692122800).

Acknowledgments

The authors greatly appreciate the valuable discussions with Bai Fan and Prof. Zhang Tao from Shanghai Institute of Ceramics, CAS.

Conflict of interest

The authors declare that the research was conducted in the absence of any commercial or financial relationships that could be construed as a potential conflict of interest.

Generative AI statement

The author(s) declare that no Generative AI was used in the creation of this manuscript.

Any alternative text (alt text) provided alongside figures in this article has been generated by Frontiers with the support of artificial intelligence and reasonable efforts have been made to ensure accuracy, including review by the authors wherever possible. If you identify any issues, please contact us.

Publisher's note

All claims expressed in this article are solely those of the authors and do not necessarily represent those of their affiliated organizations, or those of the publisher, the editors and the reviewers. Any product that may be evaluated in this article, or claim that may be made by its manufacturer, is not guaranteed or endorsed by the publisher.

References

- Abdal-hay, A., Raveendran, N. T., Fournier, B., and Ivanovski, S. (2020). Fabrication of biocompatible and bioabsorbable Polycaprolactone/Magnesium hydroxide 3D printed scaffolds: degradation and *in vitro* osteo-blasts interactions. *Compos. Part B-Engineering* 197, 108158. doi:10.1016/j.compositesb.2020.108158
- AlMangour, B., Cheng, J., Grzesiak, D., Hwang, Y.-J., and Kee-Ahn, L. (2023). Fundamental Study on the development of pure magnesium parts by additive manufacturing: an experimental and computational analysis. *Metals Mater. Int.* 29 (2), 429–443. doi:10.1007/s12540-022-01300-x
- Asadollahi, M., Alizadeh, R., Mahmudi, R., Labbaf, S., Sadrnezhaad, S. K., and Atari, M. (2024). Using solution heat treatment and multi directional forging to improve the mechanical and corrosion properties of an Mg-2Zn-0.2Ag alloy. *Metals Mate-rials Int.* 30 (6), 1538–1555. doi:10.1007/s12540-023-01602-8
- Bas, O., Hansske, F., Lim, J., Ravichandran, A., Kemnitz, E., Teoh, S. H., et al. (2019). Tuning Me-chanical reinforcement and bioactivity of 3D printed ternary nanocomposites by interfacial peptide-polymer conjugates. *Biofabrication* 11 (3), 035028. doi:10.1088/1758-5090/aafec8
- Beyzavi, A. H., Azadi, M., Dezianian, S., and Talebsafa, V. (2023). Bio-Polymer coatings fabricated on AM60 magnesium alloys by fused deposition modeling 3D-Printing to investigate electrochemical behavior. *Mater. Lett.* 337, 133935. doi:10.1016/j.matlet.2023.133935
- Bian, D., Tong, Z., Gong, G., Huang, He, Cai, G., Yan, X., et al. (2024). A spatiotemporal "Bulk Erosion" mode in selective laser melted magnesium alloys and the resulting adverse cell tissue responses. *J. Mater. Sci. Technol.* 198, 243–258. doi:10.1016/j.jmst.2024.01.075
- Cai, X., Chen, F., Dong, B., Lin, S., and Yang, C. (2024). Microstructure and mechanical properties of GTA-Based wire arc additive manufactured AZ91d magnesium alloy. *J. Magnesium Alloys* 12 (8), 3180–3192. doi:10.1016/j.jma.2022.11.018
- Cao, X., Wang, X., Chen, J., Geng, X., and Tian, H. (2024). 3D printing of a porous Zn-1Mg-0.1Sr alloy scaffold: a Study on mechanical properties, degradability, and biosafety. *J. Funct. Biomaterials* 15 (4), 109. doi:10.3390/jfb15040109
- Chen, S., Yi, H., Wang, Q., and Cao, H. (2025). Effect of ultrasonic vibration on corrosion properties of wire-arc directed energy deposited magnesium alloy. *J. Alloys Compd.* 1019, 179313. doi:10.1016/j.jallcom.2025.179313
- Elhattab, K., Bhaduri, S. B., Lawrence, J. G., and Sikder, P. (2021). Fused filament fabrication (Three-Dimensional printing) of amorphous magnesium Phosphate/Polylactic acid macroporous biocomposite scaffolds. *ACS Appl. bio Mater.* 4 (4), 3276–3286. doi:10.1021/acsabm.0c01620
- Fu, Q., Xiong, J., Zhang, C., Li, Z., Gan, J., Huang, W., et al. (2025). Effects of zinc silicate additive on the physicochemical properties and cellular behaviors of 3D-Printed magnesium phosphate Bioceramic scaffolds. *Biomed. Mater.* 20 (2), 025039. doi:10.1088/1748-605x/adbaa2
- Gneiger, S., Oesterreicher, J. A., Arnoldt, A. R., Birgmann, A., and Fehlbier, M. (2020). Development of a high strength magnesium alloy for wire arc additive manufacturing. *Metals* 10 (6), 778. doi:10.3390/met10060778
- Gu, D. D., Meiners, W., Wissenbach, K., and Poprawe, R. (2012). Laser additive manufacturing of metallic components: materials, processes and mechanisms. *Int. Mater. Rev.* 57 (3), 133–164. doi:10.1179/1743280411y.0000000014
- Guo, A. X. Y., Cheng, L., Zhan, S., Zhang, S., Xiong, W., Wang, Z., et al. (2022). Biomedical applications of the powder-based 3D printed titanium alloys: a review. *J. Mater. Sci. & Technol.* 125, 252–264. doi:10.1016/j.jmst.2021.11.084
- Han, S., Zielewski, M., Holguin, D. M., Parra, M. M., and Kim, N. (2018). Optimization of AZ91d process and corrosion resistance using wire arc additive manufacturing. *Appl. Sciences-Basel* 8 (8), 1306. doi:10.3390/app8081306
- Hartmann, C., Venkatesan, K., de Looze, G., Takashima, K., Shen, S., and Wilson, R. (2024). Additive manufacturing of WE43 and modified AZ91d magnesium alloys using the laser engineered net shaping process. *Mater. Today Commun.* 39, 108774. doi:10.1016/j.mtcomm.2024.108774
- Hendea, R. E., Raducanu, D., Claver, A., Garcia, J. A., Cojocaru, V. D., Nocivin, A., et al. (2023). Biodegradable magnesium alloys for personalised temporary implants. *J. Funct. Biomaterials* 14 (8), 400. doi:10.3390/jfb14080400
- Hu, Q., Chen, C., Liu, M., Chang, C., Yan, X., and Dai, Y. (2023). Improved corrosion resistance of magnesium alloy prepared by selective laser melting through T4 heat treatment for biomedical applications. *J. Mater. Res. Technology-JMR&T* 27, 813–825. doi:10.1016/j.jmrt.2023.09.306
- Huang, J., Qin, Q., and Wang, J. (2020). A review of stereolithography: processes and systems. *Processes* 8 (9), 1138. doi:10.3390/pr8091138
- Javadi, Y., MacLeod, C. N., Pierce, S. G., Gachagan, A., Lines, D., Mineo, C., et al. (2019). Ultrasonic phased array inspection of a Wire + Arc Additive Manufactured (WAAM) sample with intentionally embedded defects. *Addit. Manuf.* 29, 100806. doi:10.1016/j.addma.2019.100806
- Karunakaran, R., Ortgies, S., Ali, T., Bobaru, F., and Sealy, M. P. (2020). Additive manufacturing of magnesium alloys. *Bioact. Mater.* 5 (1), 44–54. doi:10.1016/j.bioactmat.2019.12.004

- Kaur, M., and Singh, K. (2019). Review on titanium and titanium based alloys as biomaterials for orthopaedic applications. *Mater. Sci. Eng. C-Materials Biol. Appl.* 102, 844–862. doi:10.1016/j.msec.2019.04.064
- Kuah, K. X., Salehi, M., Huang, Z., Zhang, Su X., Li Seet, H., Nai, M. L. S., et al. (2022). Surface modification with phosphate and hydroxyapatite of porous magnesium scaffolds fabricated by binder jet additive manufacturing. *Crystals* 12 (12), 1850. doi:10.3390/cryst12121850
- Kumar, P., Kumar Rajak, D., Abubakar, M., Ali, S. G. M., and Hussain, M. (2021a). 3D printing technology for biomedical practice: a review. *J. Mater. Eng. Perform.* 30 (7), 5342–5355. doi:10.1007/s11665-021-05792-3
- Kumar, R., Kumar, M., and Singh Chohan, J. (2021b). The role of additive manufacturing for biomedical applications: a critical review. *J. Manuf. Process.* 64, 828–850. doi:10.1016/j.jmapro.2021.02.022
- Li, Y., Zhou, J., Pavanram, P., Leeflang, M. A., Fockaert, L. I., Pouran, B., et al. (2018). Additively manufactured biodegradable porous magnesium. *Acta Biomater*. 67, 378–392. doi:10.1016/j.actbio.2017.12.008
- Li, C., Zhang, W., Nie, Y., Du, X., Huang, C., Li, L., et al. (2024). Time-Sequential and multi-functional 3D printed ${\rm MgO_2/PLGA}$ scaffold developed as a novel biode-gradable and bioactive bone substitute for challenging postsurgical osteosarcoma treatment. *Adv. Mater.* 36 (34), 2308875. doi:10.1002/adma.202308875
- Liang, W., Zhou, C., Zhang, H., Bai, J., Jiang, Bo, Jiang, C., et al. (2023). Recent advances in 3D printing of biodegradable metals for orthopaedic applications. *J. Biol. Eng.* 17 (1), 56. doi:10.1186/s13036-023-00371-7
- Lin, T., Wang, X., Jin, L., Li, W., Zhang, Y., Wang, A., et al. (2021). Manu-facturing of porous magnesium scaffolds for bone tissue engineering by 3D gel-printing. *Mater. & Des.* 209, 109948. doi:10.1016/j.matdes.2021.109948
- Lin, T., Dong, J., Wang, X., Deng, X., and Shao, H. (2023). Effect of Zn content on 3D gel-printed porous Mg-Zn scaffolds for bone engineering. *J. Mater. Sci.* 58, 1229–1242. doi:10.1007/s10853-022-08108-5
- Liu, B., Liu, J., Wang, C., Wang, Z., Min, S., Wang, C., et al. (2024a). High temperature oxidation treated 3D printed anatomical WE43 alloy scaffolds for repairing periarticular bone defects: *in vitro* and *in vivo* studies. *Bioact. Mater.* 32, 177–189. doi:10.1016/j.bioactmat.2023.09.016
- Liu, H., Yu, L., Liu, S., Yao, R., Zhang, J., Wang, W., et al. (2024b). The effects of 3D printing parameters, structural design and post-processing on the mechanical properties and corrosion resistance of SLMed ZK60 porous scaffolds. *Mater. Today Commun.* 39, 109123. doi:10.1016/j.mtcomm.2024.109123
- Long, Q., Meng, Na, Chen, F., Zhang, L., Tao, X., Liu, L., et al. (2023). Phase Equilibria and microstructure development in Mg-Rich mg-gd-sr alloys: experiments and calphad assessment. *Cal-phad-Computer Coupling Phase Diagrams Thermochem.* 82, 102583. doi:10.1016/j.calphad.2023.102583
- Mahajan, A., Singh, G., and Devgan, S. (2023). Additive manufacturing of metallic biomaterials: a concise review. *Archives Civ. Mech. Eng.* 23 (3), 187. doi:10.1007/s43452-023-00730-7
- Manakari, V., Parande, G., and Gupta, M. (2017). Selective Laser melting of magnesium and magnesium alloy powders: a review. *Metals* 7 (1), 2. doi:10.3390/met7010002
- Manjhi, S. K., Sekar, P., Bontha, S., and Balan, A. S. S. (2023). Effect of equiaxed grains and secondary phase particles on mechanical properties and corrosion behaviour of CMT- based wire Arc Additive manufactured AZ31 Mg alloy. *Cirp J. Manuf. Sci. Technol.* 46, 48–64. doi:10.1016/j.cirpj.2023.07.008
- Min, S., Wang, C., Liu, B., Liu, J., Liu, Yu, Jing, Z., et al. (2023). The biological properties of 3D-Printed degradable magnesium alloy WE43 porous scaffolds via the oxidative heat strategy. *Int. J. Bioprinting* 9 (3), 686–104. doi:10.18063/ijb.686
- Murphy, S. V., and Atala, A. (2014). 3D bioprinting of tissues and organs. *Nat. Biotechnol.* 32 (8), 773–785. doi:10.1038/nbt.2958
- Murr, L. E., Quinones, S. A., Gaytan, S. M., Lopez, M. I., Rodela, A., Martinez, E. Y., et al. (2009). Microstructure and mechanical behavior of Ti-6Al-4V produced by rapid-layer manufacturing, for biomedical applications. *J. Mech. Behav. Biomed. Mater.* 2 (1), 20–32. doi:10.1016/j.jmbbm.2008.05.004
- Nabiyouni, M., Brueckner, T., Zhou, H., Gbureck, U., and Bhaduri, S. B. (2018). Magnesium-Based bioceramics in orthopedic applications. *Acta Biomater.* 66, 23–43. doi:10.1016/j.actbio.2017.11.033
- Ng, C. C., Savalani, M. M., Lau, M. L., and Man, H. C. (2011a). Microstructure and mechanical properties of selective laser melted magnesium. *Appl. Surf. Sci.* 257 (17), 7447–7454. doi:10.1016/j.apsusc.2011.03.004
- Ng, C. C., Savalani, M., and Chung Man, H. (2011b). Fabrication of magnesium using selective laser melting tech-nique. *Rapid Prototyp. J.* 17 (6), 479–490. doi:10.1108/13552541111184206
- Ngo, T. D., Kashani, A., Imbalzano, G., Nguyen, K. T. Q., and Hui., D. (2018). Additive manufacturing (3D printing): a review of materials, methods, applications and challenges. *Compos. Part B-Engineering* 143, 172–196. doi:10.1016/j.compositesb.2018.02.012

- Parupelli, S. K., Saudi, S., Bhattarai, N., and Desai, S. (2023). 3D printing of PCL-Ceramic composite scaffolds for bone tissue engineering applications. *Int. J. Bioprinting* 9 (6), 539–551. doi:10.36922/ijb.0196
- Qin, Yu, Wen, P., Guo, H., Xia, D., Zheng, Y., Jauer, L., et al. (2019). Additive manufacturing of biodegradable metals: current research status and future perspectives. *Acta Biomater.* 98, 3–22. doi:10.1016/j.actbio.2019.04.046
- Ren, X., Shao, H., Lin, T., and Zheng, H. (2016). 3D gel-printing-an additive manufacturing method for producing complex shape parts. *Mater. Des.* 101, 80–87. doi:10.1016/j.matdes.2016.03.152
- Rezanezhad, S., and Azadi, M. (2024). The influence of 3D-Printed PIA coatings on pure and fretting fatigue prop-erties of AM60 magnesium alloys under cyclic bending loads. *Heliyon* 10 (8), e29552. doi:10.1016/j.heliyon.2024.e29552
- Roseti, L., Parisi, V., Petretta, M., Cavallo, C., Desando, G., Bartolotti, I., et al. (2017). Scaffolds for bone tissue engineering: state of the art and new perspectives. *Mater. Sci. Eng. C-Materials Biol. Appl.* 78, 1246–1262. doi:10.1016/j.msec.2017.05.017
- Salehi, M., Maleksaeedi, S., Sapari, M. A. B., Nai, M. L. S., Meenashisundaram, G. K., and Gupta, M. (2019). Additive manufacturing of magnesium-zinc-zirconium (ZK) alloys *via* capillary-mediated binderless three-dimensional printing. *Mater. Des.* 169, 107683. doi:10.1016/j.matdes.2019.107683
- Salehi, M., Xiang Kuah, K., Ho, J. H., Zhang, Su X., Seet, H.Li, and Nai, M. L. S. (2023a). Towards binder jetting and sintering of AZ91 magnesium powder. *Crystals* 13 (2), 286. doi:10.3390/cryst13020286
- Salehi, M., Xiang Kuah, K., Huang, Z., Blackwood, D. J., Zhang, Su X., Seet, H.Li, et al. (2023b). Enhancing densification in binder jet additive manufacturing of magnesium *via* nanoparticles as sintering aids. *J. Manuf. Process.* 99, 705–717. doi:10.1016/j.jmapro.2023.05.096
- Salehi, M., Neo, D. W. K., Rudel, V., Stautner, M., Ganser, P., Zhang, S. X., et al. (2024). Digital manufacturing of Personalized Magnesium implants through Binder jet additive manufacturing and automated post machining. *J. Magnesium Alloys* 12 (8), 3308–3324. doi:10.1016/j.jma.2024.07.027
- Salehi, M., Xiang Kuah, K., Prasadh, S., Li, Y., Zhang, Su X., Seet, H.Li, et al. (2025). Achieving biomimetic porosity and strength of bone in magnesium scaffolds through Binder jet additive manufacturing. *Biomater. Adv.* 166, 214059. doi:10.1016/j.bioadv.2024.214059
- Shao, H., Zhang, Y., Lin, T., Peng, J., Wang, A., Yu, F., et al. (2020). Effect of $\rm Mg^{2+}$ on porous $\rm MgXCa_{3-X}(PO_4)_2$ composite scaffolds for bone engineering by 3D gel-printing. *J. Mater. Sci.* 55 (18), 7870–7882. doi:10.1007/s10853-020-04590-x
- Sheng, X., Wang, Ao, Wang, Z., Liu, He, Wang, J., and Chen, Li (2022). Advanced surface modification for 3D-Printed titanium alloy implant interface functionalization. *Front. Bioeng. Biotechnol.* 10, 850110. doi:10.3389/fbioe.2022.850110
- Sing, S. L., Jia, An, Yeong, W. Y., and Wiria, F. E. (2016). Laser and electron-beam powder-bed additive manufacturing of metallic implants: a review on processes, materials and designs. *J. Orthop. Res.* 34 (3), 369–385. doi:10.1002/jor.23075
- Tetsuka, H., and Shin, Su R. (2020). Materials and technical innovations in 3d printing in biomedical applications. *J. Mater. Chem. B* 8 (15), 2930–2950. doi:10.1039/d0tb00034e
- Vandenbroucke, B., and Kruth, J.-P. (2007). Selective Laser melting of biocompatible metals for rapid manufacturing of medical parts. *Rapid Prototyp. J.* 13 (4), 196–203. doi:10.1108/13552540710776142
- Wang, X., Xu, S., Zhou, S., Xu, W., Leary, M., Choong, P., et al. (2016). Topological design and additive manufacturing of porous metals for bone scaffolds and orthopaedic implants: a review. *Biomaterials* 83, 127–141. doi:10.1016/j.biomaterials.2016.01.012

- Wu, C. L., Zai, W., and Man, H. C. (2021). Additive manufacturing of ZK60 Magnesium alloy by selective laser melting: parameter optimization, microstructure and biodegradability. *Mater. Today Commun.* 26, 101922. doi:10.1016/j.mtcomm.2020.101922
- Xie, W., Wu, C., Man, H., and Chan, C. (2023). Effect of zinc content on powder characteristics, porosity, microstructure, and corrosion behavior of SLM-Printed ${\rm Mg}_{-{\rm X}}{\rm Zn}_{-0.2}{\rm Mn}$ alloys for biomedical applications. *Coatings* 13 (11), 1876. doi:10.3390/coatings13111876
- Xie, W., Man, H.-C., and Chan, C.-W. (2024). Interplay of laser power and pore characteristics in selective laser melting of ZK60 Magnesium alloys: a Study based on *in-situ* monitoring and image analysis. *J. Magnesium Alloys* 12 (4), 1346–1366. doi:10.1016/j.jma.2023.11.005
- Yang, H., Wang, L., Feng, Y., Zhao, S., and Guo, E. (2025). Deposition process optimization of mg-nd-zn-zr magnesium alloy fabricated by wire arc additive manufacturing. *Mater. Lett.* 386, 138242. doi:10.1016/j.matlet.2025.138242
- Yao, X., Tang, J., Zhou, Y., Atrens, A., Dargusch, M. S., Wiese, B., et al. (2021). Surface modification of biomedical Mg-Ca and mg-zn-ca alloys using selective laser melting: corrosion behaviour, microhardness and biocompatibility. *J. Magnesium Alloys* 9 (6), 2155–2168. doi:10.1016/j.jma.2020.08.011
- Yao, X. Y., Tang, J. C., Zhou, Y. H., Huang, Z. Z., Xu, J. B., Long, Y., et al. (2022). Selective Laser melting of an Mg/Metallic glass hybrid for significantly improving chemical and mechanical performances. *Appl. Surf. Sci.* 580, 152229. doi:10.1016/j.apsusc.2021.152229
- Yi, H., Wang, Q., and Cao, H. (2022). Wire-Arc directed energy deposition of magnesium alloys: microstructure, properties and quality optimization strategies. *J. Mater. Res. Technol.* 20, 627–649. doi:10.1016/j.jmrt.2022.07.083
- Ying, T., Zhao, Z., Yan, P., Wang, J., and Zeng, X. (2022). Effect of fabrication parameters on the micro-structure and mechanical properties of wire Arc additive manufactured AZ61 alloy. *Mater. Lett.* 307, 131014. doi:10.1016/j.matlet.2021.131014
- Yu, L., Liu, H., Li, Z., Li, W., Zhao, Y., Zhang, J., et al. (2024). Microstructure, Mechanical properties, and corrosion resistance of porous bio Mg alloy scaffolds prepared *via* a novel method. *Adv. Eng. Mater.* 26 (23), 2401382. doi:10.1002/adem.202401382
- Zhai, Y., Zhang, H., Wang, J., and Zhao, D. (2023). Research progress of metal-based additive manufacturing in medical implants. *Rev. Adv. Mater. Sci.* 62 (1), 20230148. doi:10.1515/rams-2023-0148
- Zhang, L.-C., and Attar, H. (2016). Selective Laser melting of Titanium alloys and Titanium Matrix composites for biomedical applications: a review. *Adv. Eng. Mater.* 18 (4), 463–475. doi:10.1002/adem.201500419
- Zhang, T., Mei, Li, Zhang, J., and Li, J. (2025). A stepwise sintering process for magnesium alloys fabricated by Binder Jetting additive manufacturing. *J. Alloys Compd.* 1020, 179498. doi:10.1016/j.jallcom.2025.179498
- Zhao, Ze, Zhang, T., Yang, Q., Li, M., and Li, J. (2025). Sintering and densification mechanism of SiC particle reinforced AZ91d magnesium matrix composite materials owing binder jetting. *Powder Technol.* 452, 120609. doi:10.1016/j.powtec. 2025.120609
- Zhu, Y., Guo, S., Ravichandran, D., Ramanathan, A., Taylor Sobczak, M., Sacco, A. F., et al. (2025). 3d-Printed polymeric biomaterials for health applications. *Adv. Healthc. Mater.* 14 (1), 2402571. doi:10.1002/adhm.202402571
- Zuo, X., Zhang, W., Chen, Yi, Oliveira, J. P., Zeng, Z., Yang, Li, et al. (2022). Wire-Based directed energy deposition of Nitita shape memory alloys: microstructure, phase transformation, electrochemistry, X-Ray visibility and mechanical properties. *Addit. Manuf.* 59, 103115. doi:10.1016/j.addma.2022.103115